JACS
JOURNAL OF THE AMERICAN CHEMICAL SOCIETY
pubs.acs.org/JACS
Article

The Binding Affinities of Serum Proteins to Nanoparticles

Published as part of Journal of the American Chemical Society special issue "Nano-Biomaterials for Tissue Interactions and Therapeutics".

Benjamin P. Stordy,[⋈] Zahra Sepahi,[⋈] Gabriel D. Patrón, Wei Yang, Alexander D. Goodson, Colin Blackadar, Anthony J. Tavares, Guanyou Lin, Ayden Malekjahani, Bill Ling, Rashmi Ravichandran, Derrick R. Hicks, Mikhail G. Shapiro, Miqin Zhang, Neil P. King, David Baker, Luis A. Ricardez-Sandoval, and Warren C. W. Chan[*]

Cite This: *J. Am. Chem. Soc.* 2025, 147, 20475−20492

Read Online

ABSTRACT: Nanoparticles can be coated with targeting ligands to deliver medical agents to specific cells. Serum protein adsorption affects the binding of nanoparticles to target cells. We hypothesized that serum proteins and target receptors compete for binding to nanoparticles. We tested the serum protein binding affinity of 251 nanoparticle designs. Here, we discovered that the binding affinities of serum proteins and receptors to a nanoparticle determine whether it can bind to target cells. We developed and validated a quantitative metric, the binding ratio, to identify nanoparticle designs that can bind to targets in serum with 90% sensitivity and 88% specificity. Using the binding ratio as a numerical guideline for nanoparticle design enabled us to improve the efficiency of nanoparticle binding to target cellular receptors.

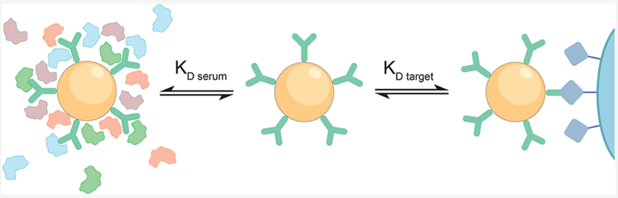

■ INTRODUCTION

Nanoparticles can be engineered to bind to specific cells for the targeted delivery of diagnostic or therapeutic cargo. There are currently no clinically approved nanoparticle targeting formulations, leading researchers to investigate the potential cause.[1] It was discovered that serum protein adsorption can interfere with nanoparticle targeting by blocking targeting ligands from recognizing their receptors. Salvati et al. showed transferrin-conjugated silica nanoparticles lose their ability to bind to transferrin receptors on cells in serum.[2] Mirshafiee et al. showed serum proteins block bicyclononyne-conjugated nanoparticles from binding to azide substrates.[3] Researchers found that changing the nanoparticle design led to improved binding to target receptors. Dai et al. demonstrated that herceptin-coated gold nanoparticles can still bind to their cellular receptors in serum when backfilled with polyethylene glycol (PEG) polymer.[4] Stordy et al. showed antibodies conjugated on gold nanoparticles coated with equilibrated serum proteins can bind to cellular receptors.[5] These studies show that serum protein adsorption affects nanoparticle targeting to varying magnitudes across different designs. No guidelines have been established to explain the variability in the nanoparticle-target binding.

A mathematical model of nanoparticle binding to target receptors in serum would allow us to understand and control nanoparticle targeting. We hypothesized that nanoparticle targeting is a competition between binding to serum proteins and to target receptors. A similar hypothesis was proposed by Dell'Orco et al., who conducted an *in silico* simulation of a single nanoparticle design binding to a target receptor and three different proteins.[6] Their simulated data suggested that the target receptor binding affinity affected nanoparticle-target binding in the presence of these three proteins. There are no existing models that account for the impact of all serum proteins on nanoparticle-target binding nor are there models that can be applied to multiple nanoparticle designs.

We sought to test our hypothesized competition experimentally with whole serum using different nanoparticle designs. Testing our model requires a quantitative measurement of serum protein binding and target protein binding for each nanoparticle design. The equilibrium dissociation constant provides a quantitative measure of the protein binding affinity. Figure 1 shows the overall experimental workflow. Here, we measured the serum protein binding affinity and target protein binding affinity for a library of 251 nanoparticle designs. These measurements provide data to build, test, and experimentally validate a model to predict

Received: February 11, 2025
Revised: April 28, 2025
Accepted: April 29, 2025
Published: June 9, 2025

ACS Publications

https://doi.org/10.1021/jacs.5c02576
J. Am. Chem. Soc. 2025, 147, 20475−20492

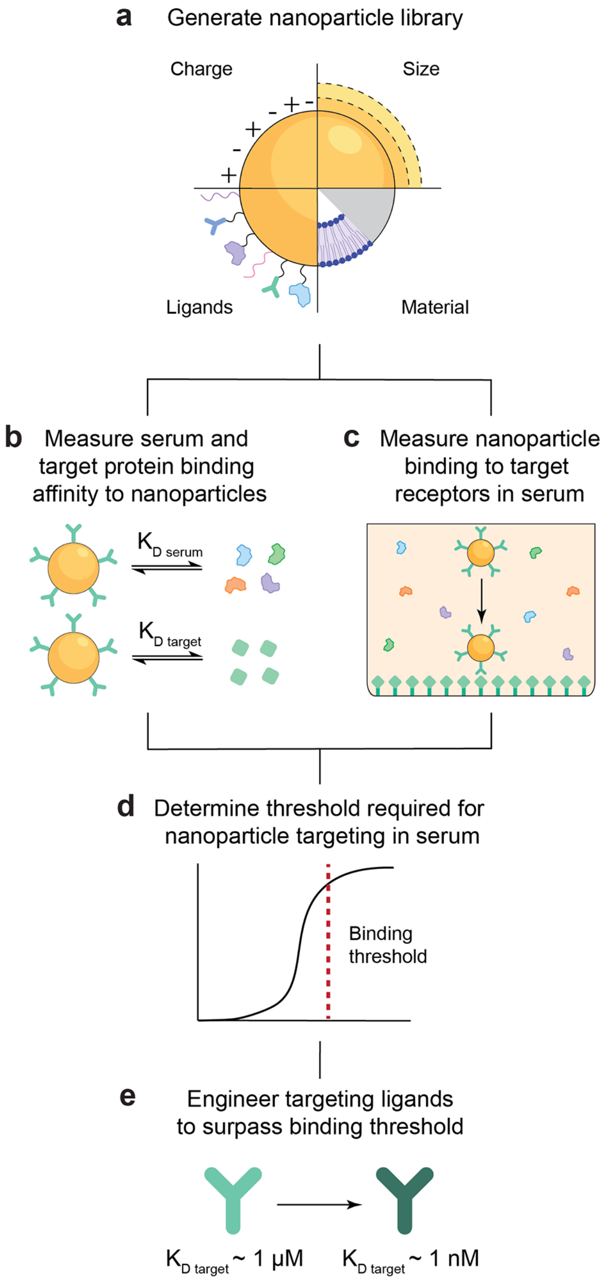

Figure 1. Schematic of the experimental workflow. (a) Generate a library of nanoparticles with varying size, charge, material, and surface ligands. (b) Measure the nanoparticle-serum protein binding affinity and nanoparticle-target protein binding affinity using biolayer interferometry. (c) Measure nanoparticle binding to target receptors in serum to analyze the competition between serum proteins and target receptors for nanoparticle binding. (d) Determine the binding threshold required for nanoparticles to achieve target binding in serum. (e) Engineer high target protein binding affinity ligands for nanoparticles to surpass the binding threshold and achieve efficient targeting in serum.

which nanoparticle designs will bind to target receptors in serum. The binding equation provides a general design metric to engineer nanoparticles for efficient targeting.

■ RESULTS AND DISCUSSION

Generating a Library of 251 Nanoparticle Designs. We used a combinatorial approach to generate a library of 251 nanoparticle designs for evaluating the binding of serum proteins to nanoparticles. The designs spanned a wide range of physicochemical properties, including material, size, surface charge, and surface chemistry. These properties have previously been demonstrated to alter serum protein and cellular interactions of nanoparticles.[2,7,8] We tested nanoparticles made from lipids, proteins (gas vesicles, adeno-associated virus, and virus-like particles), polymers, iron oxide, gold, and silica. The nanoparticles varied in size from 20 to 300 nm. The surface charge of the nanoparticles varied from under −50 to over +10 mV. We modified the surface chemistry by conjugating oligonucleotides, antibodies, proteins, and polymers to the nanoparticles. The nanoparticles were characterized using dynamic light scattering to measure the diameter, polydispersity index, and surface charge (see Supporting Information spreadsheet). Our library also includes designs that are chemically similar to Doxil anticancer liposomes, Comirnaty COVID-19 lipid nanoparticle vaccines, and Feraheme iron oxide nanoparticles.[9−13]

Measuring the Nanoparticle Serum Protein Binding Affinity. We define the nanoparticle serum protein binding affinity as the equilibrium dissociation constant of serum proteins with respect to nanoparticles. Cao et al. measured the equilibrium association constant of mouse serum to eight different polymeric-based nanoparticles using isothermal titration calorimetry and microscale thermophoresis.[14] Cedervall et al. measured the serum protein equilibrium dissociation constant of two different polymeric nanoparticle designs using surface plasmon resonance and isothermal titration calorimetry.[15] Hühn et al. conducted a meta-analysis of over 130 data sets where different instruments measured the equilibrium dissociation constants of single proteins to nanoparticles.[16] Despite these studies, it was difficult to reach definitive conclusions to guide future nanoparticle designs. Each study measured the binding affinity of different protein samples to different nanoparticles using different instruments, making it impossible to compare values. We considered these techniques, but each can only be applied to a limited set of nanoparticle designs.[15−18] We used biolayer interferometry, because it enables us to measure the serum protein binding affinity of all nanoparticle designs. It can be performed *in situ* and at high throughput.

Biolayer interferometry measures the optical thickness shift on a biosensor tip, yielding kinetic measurements from which rate constants can be determined.[19] Biolayer interferometry can measure the binding affinity of specific ligand−protein interactions. We adapted this technique and optimized a protocol to measure the binding affinity of serum proteins and receptors for all nanoparticle designs. Measuring the serum protein binding affinity to the nanoparticle surface included six steps (Figure 2a). First, we loaded the nanoparticles to the streptavidin-coated biosensors using biotin−streptavidin chemistry. We attached biotin to the nanoparticle surface. For gold nanoparticles, we used gold−thiol chemistry to attach biotin-poly(ethylene glycol) (PEG)-thiol (SH) at a low density onto the surface. We verified that the biotin did not affect the serum protein interaction measurements by measuring the adsorbed proteins on the nanoparticles using sodium dodecyl sulfate polyacrylamide gel electrophoresis (SDS-PAGE) and bicinchoninic acid assay (BCA) (Figure S1).[5] For lipid nanoparticles and liposomes, we incorporated biotin-PEG-1,2-distearoyl-*sn*-glycero-3-phosphoethanolamine (biotin-PEG-DSPE) lipids into the nanoparticles during synthesis. For

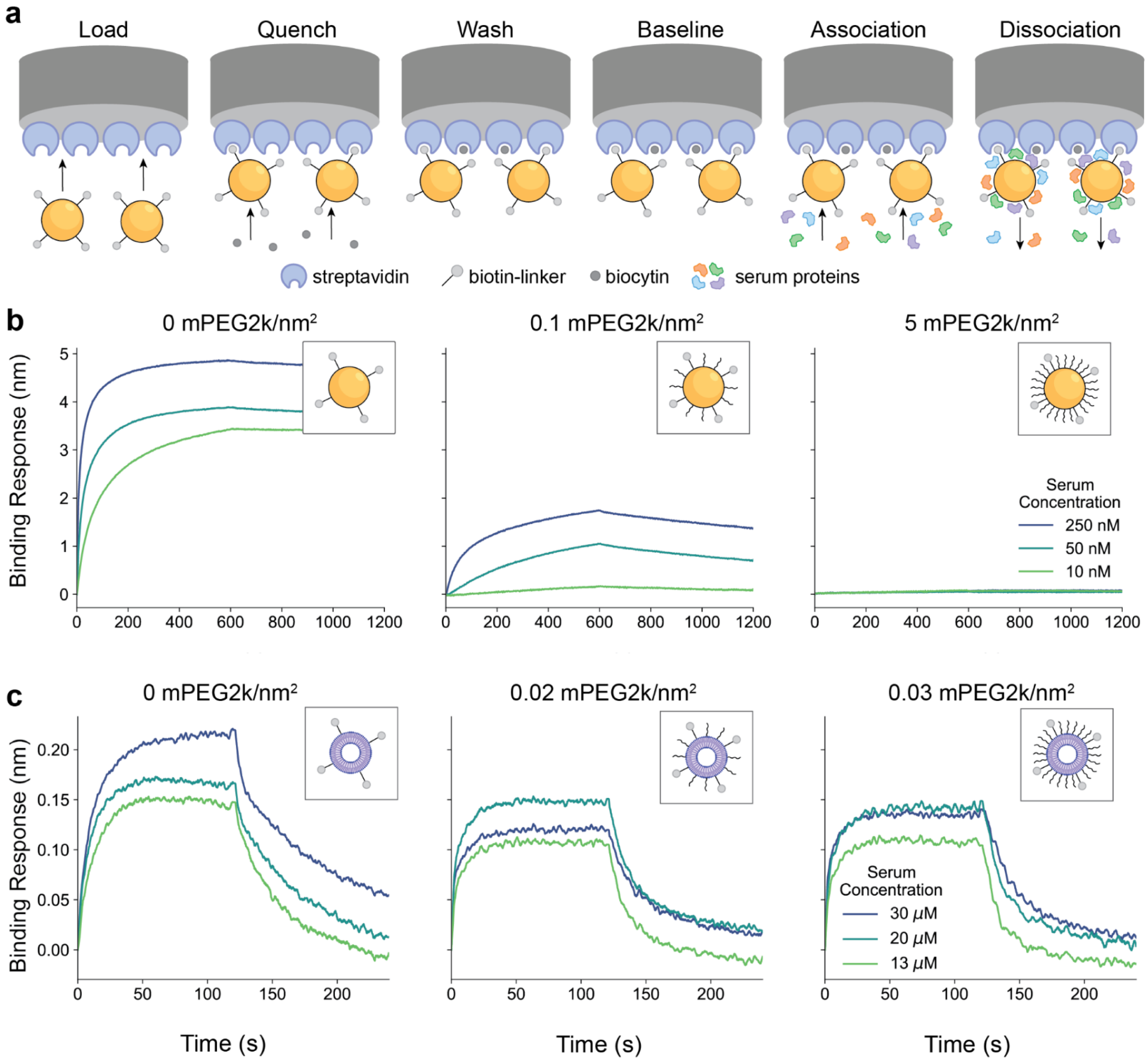

Figure 2. Biolayer interferometry measures the serum protein binding affinities to different nanoparticle designs. (a) Schematic showing the workflow of the biolayer interferometry for nanoparticle-serum protein binding measurements. Biotin-tagged nanoparticles were loaded to streptavidin coated biosensors. The unbound streptavidin was quenched with biocytin (gray circles) to reduce nonspecific binding. Unbound nanoparticles were washed off with a buffer solution consisting of either 10 mM phosphate with 20 mM NaCl and 0.02% Tween 20 for gold, silica, polystyrene, polymer, and protein nanoparticles, or 1× phosphate buffered saline with 0.005% Tween 20 for liposomes and lipid nanoparticles. The biosensor was moved into the buffer to establish a baseline signal. The biosensor was transferred into human serum protein diluted in the buffer with concentrations ranging from 2 to 3000 nM. We measured the protein association to nanoparticles, then back into the buffer to measure protein dissociation. (b) Biolayer interferometry graphs showing the association and dissociation of serum proteins to gold nanoparticles coated with 0, 0.1, and 5 mPEG2k/nm^2 densities at serum concentrations of 250 (blue line), 50 (teal line), and 10 nM (green line). (c) Biolayer interferometry graphs showing the association and dissociation of serum proteins to liposomes with 0, 0.02 , and 0.03 mPEG2k/nm^2 densities at serum concentrations of 30 (blue line), 20 (teal line), and 13 μM (green line).

poly lactic-*co*-glycolic acid polymer nanoparticles, we incorporated poly(lactide-*co*-glycolide)-*b*-poly(ethylene glycol)-biotin polymers into the nanoparticles during synthesis. For protein-based nanoparticles such as gas vesicles and adeno-associated viruses, we used amine-*N*-hydroxysuccinimide (NHS) ester chemistry to attach biotin-PEG-NHS onto the nanoparticle surface. For iron oxide, silica, and polystyrene nanoparticles, we used amine-NHS chemistry to attach biotin-PEG-NHS to the amine-functionalized nanoparticle surfaces. For virus-like particles, biotin-functionalized proteins were incorporated into the nanoparticle structure during synthesis. Second, we quenched the unbound streptavidin on the biosensor with biocytin to reduce the level of nonspecific binding of serum proteins to the biosensor surface. Third, we rinsed the biosensor with a buffer solution to remove any unbound nanoparticles. The buffer consisted of either 10 mM phosphate with 20 mM NaCl and 0.02% Tween 20 for gold nanoparticles or 1× phosphate buffered saline with 0.005% Tween 20 for liposomes. Fourth, we obtained a baseline measurement by moving the biosensor into the buffer. Fifth, we transferred the biosensor to different concentrations of serum proteins and measured their adsorption to the nanoparticles. For each nanoparticle design, we selected serum concentrations that produced binding curves that ranged between near saturation

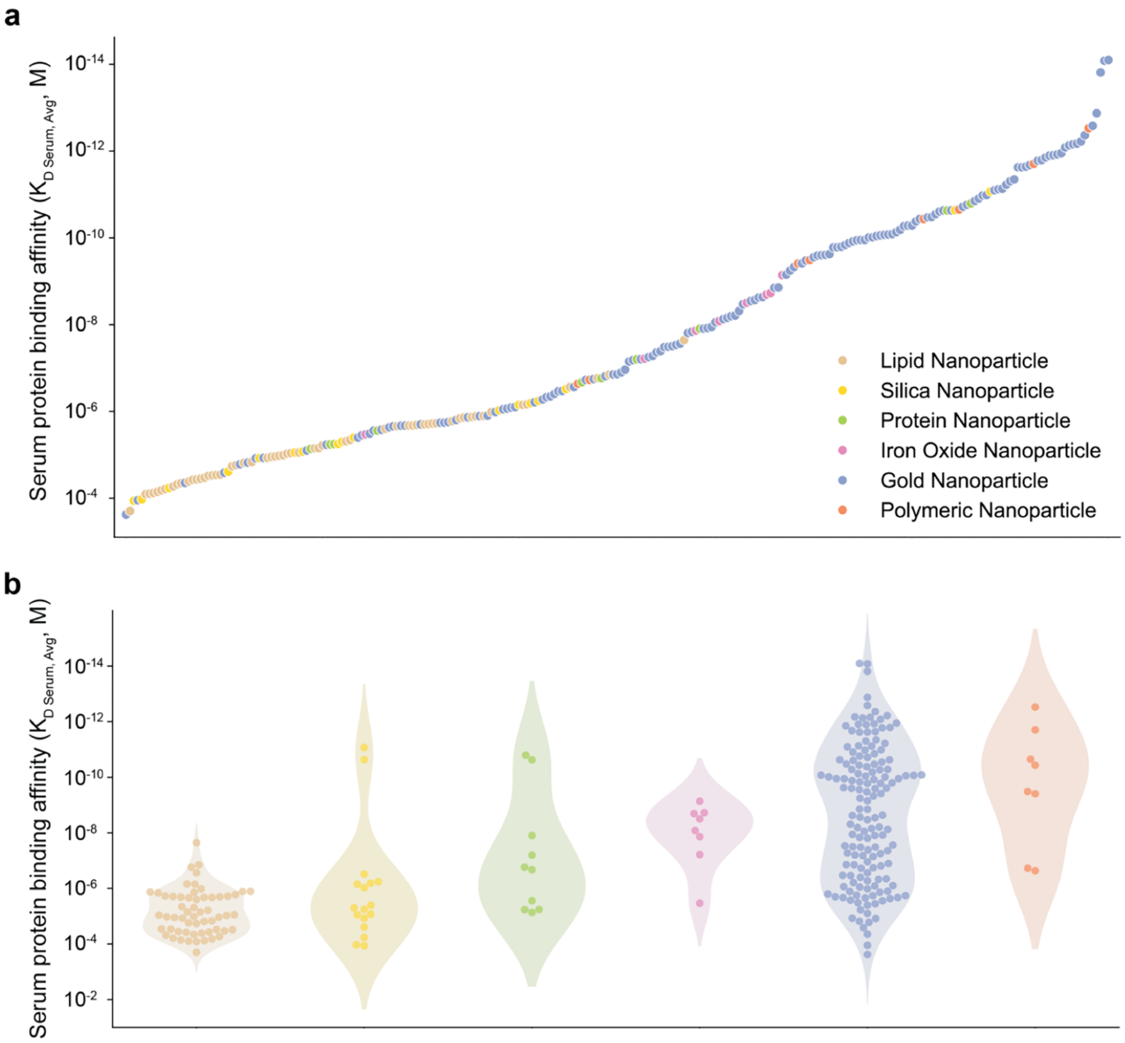

Figure 3. Nanoparticle-serum protein binding affinities vary by more than 7 orders of magnitude across the nanoparticle library. (a) Serum protein binding affinity ($K_{D,\mathrm{avg}}$) ranked from weakest to strongest binding affinity for 251 nanoparticle designs with six different chemical compositions. Lipid nanoparticles are shown in brown (n = 58), silica nanoparticles are shown in yellow (n = 17), protein nanoparticles are shown in green (n = 9), iron oxide nanoparticles are shown in pink (n = 8), gold nanoparticles are shown in blue (n = 150), and polymer nanoparticles are shown in orange (n = 8). Between three and five human serum protein concentrations were used to measure the serum protein binding affinity of each nanoparticle. (b) Comparison of the average serum protein binding affinities ($K_{D,\mathrm{avg}}$) of nanoparticles grouped by chemical composition. Violin plots of the probability distributions of each material type are overlaid.

and almost no binding. Sixth, we transferred the biosensor back into the buffer and measured the dissociation of serum proteins from the nanoparticle surface. We accounted for signal drift caused by nanoparticles detaching from the sensor and nonspecific protein binding to the biosensor.

Some materials, such as bare gold nanoparticles, showed large binding responses, even at low serum protein concentrations (Figure 2b). When the gold nanoparticle-coated biosensors were moved into the serum protein solution at 250 nanomolar, the binding response rapidly reached 5 nm as proteins bound to the gold nanoparticles (blue line). When the biosensors were moved into the buffer, there was only a minor signal decrease (<0.1 nm). This result indicated that the proteins did not dissociate because they were strongly bound to the gold nanoparticles. Other materials, such as liposomes, showed small binding responses at high serum concentrations (Figure 2c). When the liposome-coated biosensors were moved into the serum protein solution at 30 micromolar, the binding signal rapidly reached 0.2 nm, as proteins bound to the liposomes (blue line). When the sensors were moved into the buffer, the binding signal rapidly decreased back to 0.05 nm. This result indicated that the proteins were weakly bound to the liposomes and readily dissociated from the surface. Modifying the surface chemistry also varied the serum protein binding response. Conjugating methoxy-PEG (mPEG) polymers decreased the serum protein binding response across material types (Figure 2b,c). For mPEG conjugated-gold nanoparticles, the binding signal at 250 nanomolar only reached 0.1 nm when the biosensor moved into the serum protein solution, a 40-fold reduction in binding signal in comparison to a bare gold nanoparticle surface. The signal rapidly decreased back to 0 nm when the biosensors moved into the buffer. This result indicated that serum proteins were weakly bound to the mPEG-coated gold nanoparticles.

Obtaining Binding Rate Constants. We determined the serum protein binding affinities from the raw biolayer interferometry data. We needed to fit the data using a binding model. To accomplish this goal, we tested multiple models to perform curve fitting. We first tested a one component model. The one component model describes a 1:1 binding interaction in which one analyte binds to one ligand. We then tested a two-component model that fits a 2:1 binding interaction between two types of analytes and one ligand. The two-component model describes the binding of two populations of proteins in serum, fast-binding (soft corona) and slow-binding (hard corona), that associate to and dissociate from the nanoparticle surface eqs 1 and 2. Lundström and Cedervall et al. used a two component model to describe protein binding onto solid surfaces and protein binding onto polymeric nanoparticles.[15,20] We also tested a three-component model that fits a 3:1 binding interaction between three types of analytes and one ligand. We compared the goodness of fit of one-, two-, and three-component binding models for gold nanoparticles, liposomes, and adeno-associated viruses. There was a 40 to 95% improvement in the goodness of fit (X^2) moving from one to two component fit, but less than 6% improvement moving from two to three components (Figure S2). We wrote a Python script to process and fit the kinetic data using a two-component model, which is available on GitHub (github.com/chan-lab-code/BLI_processing_fitting).

The fit given by the model generates two sets of kinetic rate constants for each nanoparticle, corresponding to the fast and slow binding serum protein populations. Each population has its own binding parameters and weighting coefficients. The weights A and B quantify how much of the overall binding response is described by each component. P is the protein concentration, $B_{\max}$ is the theoretical maximum binding response shift, k_{on1} and k_{on2} are the rates of serum protein association, k_{off1} and k_{off2} are the rates of serum protein dissociation, t is time, and y is the binding response. The fitted parameters k_{on1}, k_{on2}, k_{off1}, k_{off2}, and A and B are listed in the Supporting Information spreadsheet.

$$\text{Association: } y = A\frac{B_{\max}}{1+\frac{k_{\mathrm{off1}}}{k_{\mathrm{on1}}[P]}}\left(1-e^{-k_{\mathrm{off1}}\cdot k_{\mathrm{on1}}\cdot[P]\cdot t}\right) + B\frac{B_{\max}}{1+\frac{k_{\mathrm{off2}}}{k_{\mathrm{on2}}[P]}}\left(1-e^{-k_{\mathrm{off2}}\cdot k_{\mathrm{on2}}\cdot[P]\cdot t}\right) \tag{1}$$

$$\text{Dissociation: } y = A\cdot y_0\cdot e^{-k_{\mathrm{off1}}\cdot t} + B\cdot y_0\cdot e^{-k_{\mathrm{off2}}\cdot t} \tag{2}$$

We used the equilibrium dissociation constant (K_D) to describe the binding affinity of serum proteins to nanoparticles (eq 3). Our two-component model generates two K_D values (K_{D1} and K_{D2}) with different associated weights (A and B). The K_{D1} value varied from 0.1 molar to 0.3 femtomolar (Figure S3a). The K_{D2} value varied from 97 micromolar to 1 femtomolar (Figure S3b). Neither of these values can summarize the serum protein binding affinity to nanoparticles on their own. We took a weighted geometric mean of the K_D values (eq 4). The weights account for the variable contributions (A,B) of the two K_D values (K_{D1} and K_{D2}). The geometric mean ($K_{D\mathrm{avg}}$) accounts for differences in orders of magnitude between binding affinities and provides the overall binding affinity of two-component systems.[21,22] This concept allowed us to compare the serum protein binding affinities of different nanoparticle designs using a single numerical metric.

$$K_D = \frac{k_{\mathrm{off}}}{k_{\mathrm{on}}} \tag{3}$$

$$K_{D\mathrm{avg}} = \exp\left(\frac{A\cdot\ln(K_{D1}) + B\cdot\ln(K_{D2})}{A+B}\right) \tag{4}$$

We found that the serum protein binding affinity ($K_{D\mathrm{avg}}$) ranged from below 10 femtomolar to above 100 micromolar across the 251 nanoparticle designs, a variation of over 11 orders of magnitude (Figure 3a, Supporting Information spreadsheet). We evaluated the range of serum protein binding affinities for each nanoparticle material type (Figure 3b). For lipid nanoparticles, the serum protein binding affinity ranged from 0.20 millimolar to 23 nanomolar (n = 58, shown in brown). For silica nanoparticles, the serum protein binding affinity ranged from 0.11 millimolar to 8.5 picomolar (n = 17, shown in yellow). For protein nanoparticles, the serum protein binding affinity ranged from 7.3 micromolar to 16 picomolar (n = 9, shown in green). For iron oxide nanoparticles, the serum protein binding affinity ranged from 3.0 micromolar to 0.72 nanomolar (n = 8, shown in pink). For gold nanoparticles, the serum protein binding affinity ranged from 0.24 millimolar to 7.9 femtomolar (n = 150, shown in blue). For polymer nanoparticles, the serum protein binding affinity ranged from 0.23 micromolar to 0.30 picomolar (n = 8, shown in orange). The serum protein affinities were correlated with size and surface charge with Pearson correlation coefficients of R = −0.33 and R = −0.26, respectively (Figure S4a,b).

Measuring the Effect of Nanoparticle Serum Protein Binding Affinity on Target Binding. Next, we determined the impact of serum protein binding affinity on nanoparticles' binding to target receptors. We developed an *in vitro* plate assay to assess the impact of serum proteins on nanoparticle ligands binding to receptors. We coated the receptors onto plates by using polyhistidine-nickel binding chemistry. The recombinant target receptors and the nonspecific binding control protein, human serum albumin, contained polyhistidine groups, which bound the proteins to the nickel-coated plate surface. We conjugated gold nanoparticles and liposomes with receptor-binding antibodies and labeled them with fluorophores. We selected antibodies that can bind to cancer cell receptors.[23−29] We conjugated antibodies for the epithelial cell adhesion molecule (EpCAM) and human epidermal growth receptor 2 (HER2) to a bare gold nanoparticle surface. We measured the number of antibodies bound to each nanoparticle design (Supporting Information spreadsheet). We mixed the nanoparticles in serum and in buffer and immediately added the solution to the wells coated with the target receptors and nonspecific protein control wells. This experiment allowed us to evaluate the direct competition between serum proteins and receptors for nanoparticle binding. The buffer consisted of either 10 mM phosphate with 20 mM NaCl and 0.02% Tween 20 for gold nanoparticles or 1× phosphate buffered saline with 0.005% Tween 20 for liposomes. We incubated these solutions for 1 h at room temperature. We then removed the nanoparticle solutions and washed off unbound nanoparticles with the buffer. We measured the signal of nanoparticles bound to receptors in buffer and serum and subtracted the signal from the control wells. We compared nanoparticle binding in the presence and absence of serum to quantify the effect of serum on nanoparticle-target receptor binding.

We measured the impact of serum on anti-EpCAM- and trastuzumab (anti-HER2)-conjugated gold nanoparticle binding to EpCAM and HER2 target receptors, respectively. The serum protein binding affinities of gold nanoparticles conjugated with anti-EpCAM and trastuzumab antibodies were 65 and 28 picomolar, and the target protein binding affinities were 0.78 and 14 picomolar, respectively. Antibody-conjugated gold nanoparticles bound specifically to target receptors compared to control proteins in serum and in buffer (Figure S5a). Anti-EpCAM-conjugated gold nanoparticles had a reduction in EpCAM target binding by 70% in serum relative to buffer (Figure 4a). The trastuzumab-conjugated gold nanoparticles exhibited a 100% reduction in target receptor binding in serum relative to that in the buffer (Figure 4b).

We hypothesized that lowering the serum protein binding affinity would improve the target binding in serum. A strategy to reduce serum protein binding is to attach mPEG onto nanoparticles.[4] Conjugating the gold nanoparticles with 1 kDa mPEG at a density of 5 PEG per nm^2 decreased the serum protein binding affinity by 6 orders of magnitude from nanomolar to micromolar. Antibody- and mPEG-conjugated gold nanoparticles bound specifically to target receptors compared to control proteins in serum and in buffer (Figure S5b). The serum protein binding affinities of gold nanoparticles conjugated with anti-EpCAM and trastuzumab antibodies were 0.15 and 2.2 μM, and the target protein binding affinities were 6.2 and 1.2 picomolar, respectively. We found that attaching mPEG to the nanoparticles allowed them to retain 50% of the target binding to EpCAM in serum and 100% target binding to HER2 in serum (Figure 4a,b).

We also tested target binding of liposomes that had similar serum protein binding affinities and target protein binding affinities to the gold nanoparticles conjugated with mPEG. We measured the number of antibodies bound to the liposomes (Supporting Information spreadsheet). Antibody-conjugated liposomes bound specifically to target receptors versus control proteins in serum and in buffer (Figure S6). Liposomes conjugated with anti-EpCAM and trastuzumab antibodies had serum protein binding affinities of 10.9 and 10.5 micromolar and target protein binding affinities of 2.0 picomolar and 7.2 nanomolar, respectively. The antibody-conjugated liposomes retained 74% of target binding to EpCAM in serum and 75% target binding to HER2 in serum (Figure 4a,b). The nanoparticles with reduced serum protein binding affinity, gold nanoparticles conjugated with mPEG and liposomes had significant improvements in target binding in serum for both EpCAM and HER2 compared with the plain gold nanoparticles with high serum protein binding affinity (Figure 4a,b).

We wanted to test how modifying the serum protein binding affinity of nanoparticles affected targeting cells in serum. We conjugated gold nanoparticles with anti-EpCAM and coated their surface with mPEG to create nanoparticles with high and low serum binding affinities. We also conjugated anti-EpCAM to liposomes. We fluorescently labeled each nanoparticle to allow us to measure binding to cells. We quantified their binding to human breast cancer cells MDA-MB-468 and MDA-MB-231. MDA-MB-468 cells have high EpCAM expression levels and MDA-MB-231 cells have low EpCAM expression.[30,31] We incubated the nanoparticles with cells for 1 h at 4 °C and measured their binding in serum and in buffer. Cellular metabolic and uptake processes are paused at this temperature enabling nanoparticle binding to be isolated from internalization.[32] We measured the degree of nanoparticle binding to cells using flow cytometry (Figure S7). Our result shows that the gold nanoparticles with high serum protein binding affinity had 11% target cell receptor binding in serum (Figure 4c). In contrast, gold nanoparticles with low serum

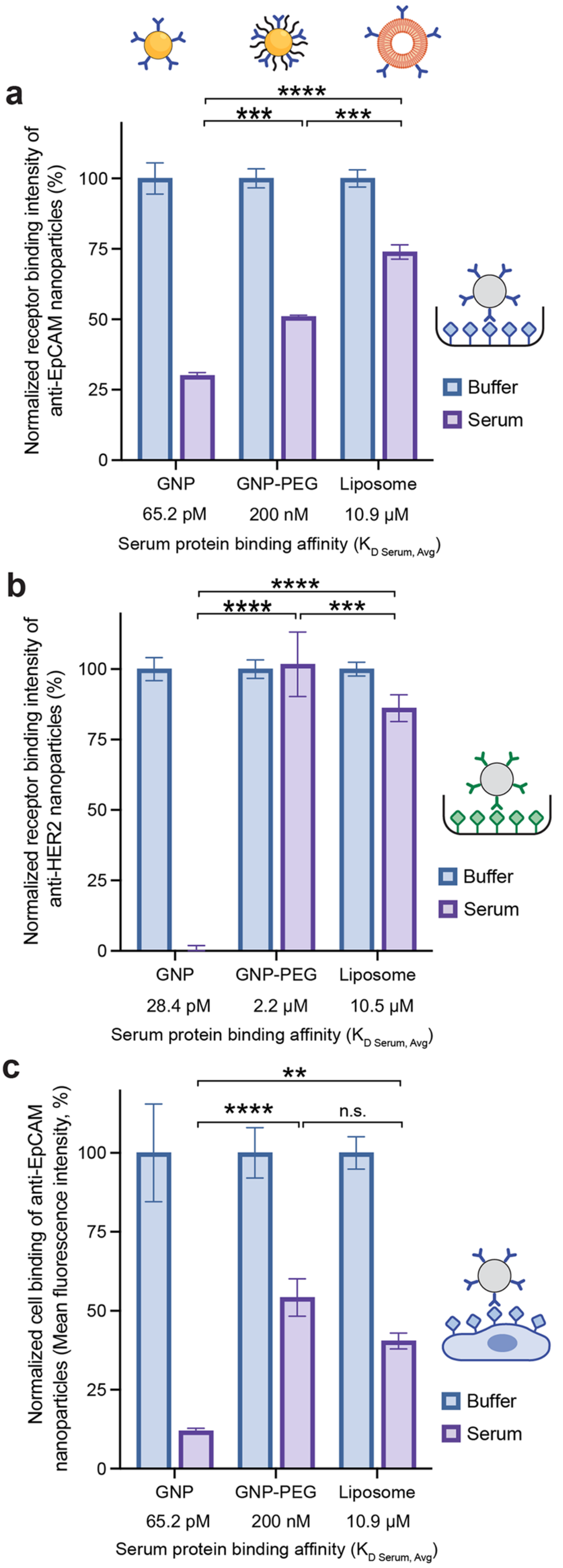

Figure 4. Serum proteins impact nanoparticle receptor binding. (a) Binding signal of AZ647 labeled gold nanoparticles, mPEG coated and AZ647 labeled gold nanoparticles, and DiO labeled liposomes

Figure 4. continued

conjugated with anti-EpCAM bound to target receptors in buffer (blue) and in 90%(v/v) human serum (purple). The binding signals were normalized to the absorbance signal of bound gold nanoparticles in a buffer solution (10 mM phosphate with 20 mM NaCl and 0.02% Tween 20) or the fluorescence signal of bound liposomes in a buffer solution (1× PBS and 0.005% Tween 20). Statistical significance was evaluated using one-way ANOVA, corrected for multiple comparisons with the Holm−Šidák method. ***$p < 0.001$, ****$p < 0.0001$. Exact p values from left to right: $p = 0.0005$, $p < 0.0001$, $p = 0.0004$. (b) Binding signal of gold nanoparticles, mPEG-coated gold nanoparticles, and liposomes conjugated with trastuzumab (anti-HER2) bound to target receptors in buffer (blue) and in 90%(v/v) human serum (purple). The binding signals were normalized to the absorbance signal of bound gold nanoparticles in the buffer (10 mM phosphate with 20 mM NaCl and 0.02% Tween 20) or the fluorescence signal of bound liposomes in the buffer (1× PBS and 0.005% Tween 20). Statistical significance was evaluated using one-way ANOVA, corrected for multiple comparisons with the Holm−Šidák method. **$p < 0.005$, ****$p < 0.0001$. Exact p values from left to right: $p < 0.0001$, $p < 0.0001$, $p = 0.004$. (c) Binding signal of gold nanoparticles, mPEG coated gold nanoparticles, and liposomes conjugated with anti-EpCAM bound to target MDA-MB-468 human breast cancer cells in buffer (blue) and in 90%(v/v) human serum (purple). The binding signals were normalized to the AZ647 fluorescence intensity of bound nanoparticles in the buffer. Statistical significance was evaluated using one-way ANOVA, corrected for multiple comparisons with the Holm−Šidák method. **$p < 0.005$, ****$p < 0.0001$. Exact p values from left to right: $p < 0.0001$, $p < 0.0016$, $p = 0.054$.

protein binding affinity had a 5-fold improvement in nanoparticle targeting with 55% of target cell receptor binding in serum. We then tested the binding of anti-EpCAM-conjugated liposomes to the same cells. The liposomes with low serum protein binding affinity had 40% binding to target cell receptors in serum, significantly more than the plain gold nanoparticles with high serum protein binding affinity and similar to the PEG-coated gold nanoparticles with low serum protein binding affinity (Figure 4c).

Predicting Nanoparticle-Target Binding in Serum. We wanted to determine the mathematical relationship that governs how the affinities of serum proteins and targets to nanoparticles impact nanoparticle-target binding in serum. We selected 33 nanoparticle targeting designs that span a wide design space with different serum protein affinities and target affinities, which we measured using biolayer interferometry. We quantified nanoparticle binding to target receptors in serum using our *in vitro* plate assay. We hypothesized that there could be three models describing the process of nanoparticle binding to target receptors in serum. In the first model, serum protein binding affinity is the sole parameter that governs nanoparticle-target binding in serum (Figure S8a). In the second model, target protein binding affinity is the sole parameter that governs nanoparticle-target binding in serum (Figure S8b). We used the coefficient of determination, R^2, to evaluate which of the three hypothesized models best explains nanoparticle-target binding in serum. An R^2 of zero indicates that the model explains the variance in the data and the mean of the data. A negative R^2 indicates that the model provides a worse explanation of the variance than the mean. An R^2 of 1 means that the model perfectly explains the variation in the data. Neither of the models that evaluated nanoparticle-target binding in serum as a function of either serum protein binding affinity or targeting binding affinity alone could adequately describe the data. We found that serum protein binding affinity was not correlated with nanoparticle receptor binding, with a coefficient of determination of $R^2 = -1.13$ (Figure S8c). Similarly, we found that target receptor binding affinity is not correlated with nanoparticle-target binding, with a coefficient of determination of $R^2 = -1.59$ (Figure S8d). These negative R^2 values demonstrate that the serum protein and target protein binding affinities on their own provide a worse description of nanoparticle targeting than the assumption of a fixed mean value.

We hypothesized a third model, where serum protein and target receptors compete for nanoparticle binding (Figure 5a and eq 5). We describe this competition for nanoparticle binding through coupled equilibria and associated dissociation constants:

$$N + S \rightleftharpoons NS\ ;\ N + T \rightleftharpoons NT \tag{5}$$

$$K_{D\text{serum}} = \frac{[N][S]}{[NS]} \tag{6}$$

$$K_{D\text{target}} = \frac{[N][T]}{[NT]} \tag{7}$$

where N, S, and T represent nanoparticles, serum proteins, and target receptors, respectively. We can rearrange these equations to determine whether nanoparticles will bind preferentially to target receptors or to serum proteins, expressed as the ratio of target-bound nanoparticles to serum-bound nanoparticles (eq 8):

$$\text{Binding Ratio} = \frac{[NT]}{[NS]} = \frac{[T]K_{D\text{serum}}}{[S]K_{D\text{target}}} \tag{8}$$

We plotted nanoparticle binding to targets as a function of the binding ratio (Figure 5b). The data followed a sigmoidal pattern. To model this behavior, we developed an equation (eq 9) to describe nanoparticle binding to targets $\left(\frac{[NT]}{[N_{\text{total}}]}\right)$ from the equilibrium dissociation constants for serum and targets (eqs 6 and 7) and the law of conservation of mass, $[N_{\text{total}}] = [N] + [NS] + [NT]$

$$\text{Nanoparticle target binding} = \frac{[NT]}{[N_{\text{total}}]} = \frac{[T]}{K_{D\text{target}}\left(1 + \frac{[T]}{K_{D\text{target}}} + \frac{[S]}{K_{D\text{serum}}}\right)} \tag{9}$$

We found that the binding ratio $\left(\frac{[T]K_{D\text{serum}}}{[S]K_{D\text{target}}}\right)$ correlated with nanoparticle receptor binding, with a coefficient of determination of $R^2 = 0.36$ (Figure 5b). This value demonstrates that modeling nanoparticle-target interactions as a combination of both serum protein binding affinity and target protein binding affinity significantly improves the goodness-of-fit. The goodness-of-fit does not indicate predictive power.

As R^2 only reflects goodness-of-fit, we sought to evaluate the ability of the binding ratio to predict nanoparticle-target binding in serum. We used sensitivity and specificity as measures of the predictive power of the binding ratio in determining whether a nanoparticle design will have low,

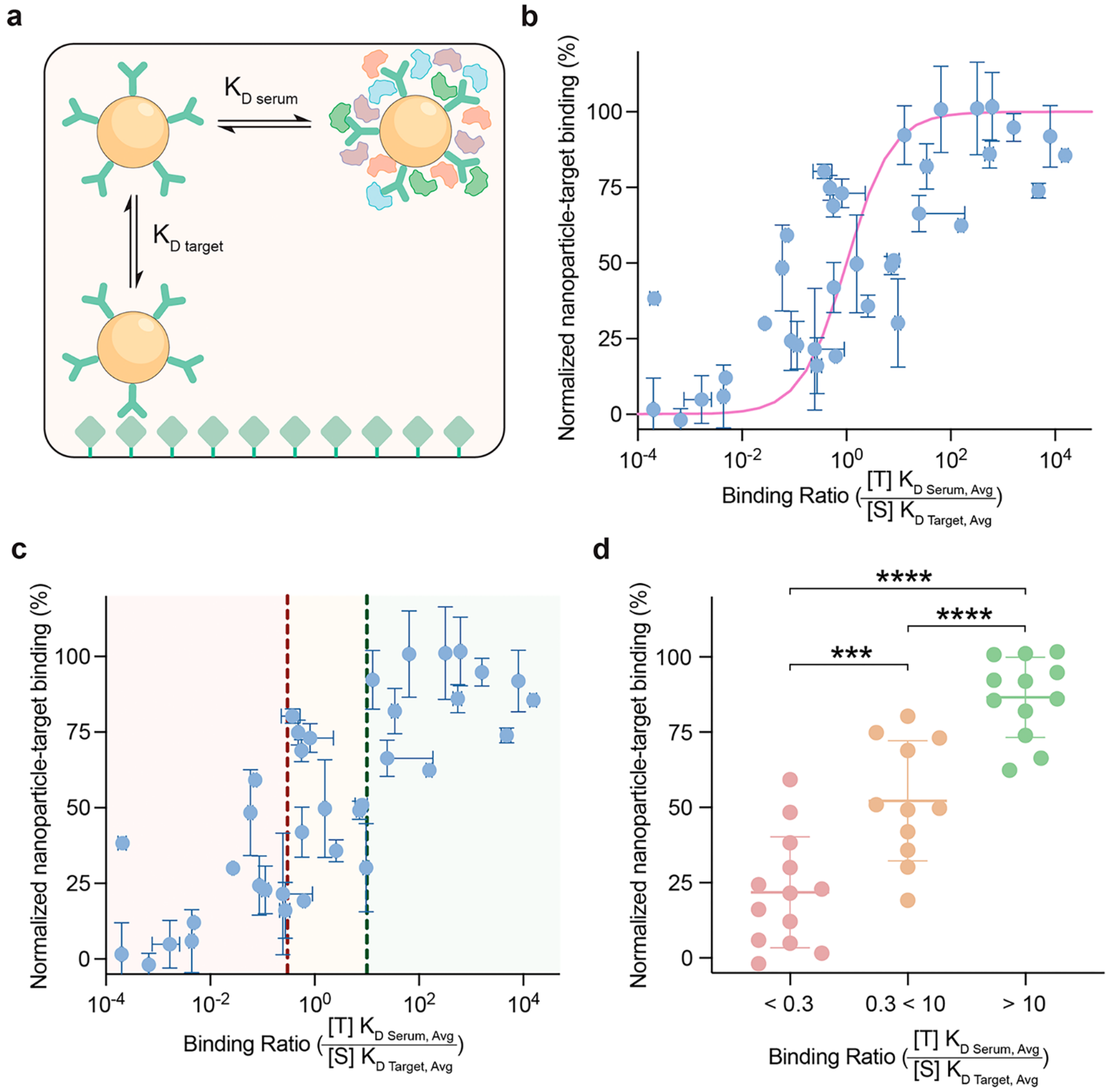

Figure 5. The binding ratio determines nanoparticle binding to targets in serum. (a) Schematic showing ligand- coated nanoparticles binding to target receptors in serum, where the serum protein binding affinity and target protein binding affinity compete to control nanoparticle binding to targets. (b) Signal of nanoparticles binding to targets in serum as a function of the binding ratio, eq 9 $\left(\frac{[T]K_{D\text{serum}}}{[S]K_{D\text{target}}}\right)$. Nanoparticle binding to targets is predicted from eq 8 $\left(y = \frac{[T]}{K_{D\text{target}}\left(1 + \frac{[T]}{K_{D\text{target}}} + \frac{[S]}{K_{D\text{serum}}}\right)}\right)$ indicated by the purple line. The correlation coefficient is $R^2 = 0.36$. (c) Threshold binding ratio values of 0.3 (red dashed line) and 10 (green dashed line) are overlaid on the plot of nanoparticles binding to targets in serum as a function of the binding ratio, eq 8 $\left(\frac{[T]K_{D\text{serum}}}{[S]K_{D\text{target}}}\right)$. (d) Comparison of nanoparticle binding to targets for nanoparticles grouped by the binding ratio. Statistical significance was evaluated using one-way ANOVA, corrected for multiple comparisons with the Holm−Šídák method. $^{**}p < 0.01$, $^{****}p < 0.0001$. Exact p values from left to right: $p = 0.0031$, $p < 0.0001$, $p < 0.0001$.

moderate, and high levels of target binding in serum. We classified low nanoparticle target binding in serum as less than 25%, moderate as between 25 and 50%, and high as greater than 75%. Low target binding nanoparticles with a binding ratio below 0.3 were identified with 85% sensitivity and 90% specificity (Figure S9). High target binding nanoparticles with a binding ratio threshold of 10 were identified with 90% sensitivity and 88% specificity (Figure S9). Nanoparticles with a binding ratio below 0.3 were predicted to have a low target binding ability in serum, with an average target binding signal of 22%. Nanoparticles with a binding ratio between 0.3 and 10 were predicted to have moderate target binding ability in serum, with an average target binding signal of 52% (Figure 5c,d). Nanoparticles with a binding ratio greater than 10 had a high target binding ability in serum and were predicted to have an average target binding signal of 87% (Figure 5d). This result demonstrated that the binding ratio can effectively predict nanoparticle binding to target receptors in serum. The binding ratio is a quantitative guideline for designing nanoparticles and selecting targeting ligands.

Ligands Engineered for Increased Target Receptor Binding. A strategy to increase the binding threshold in favor

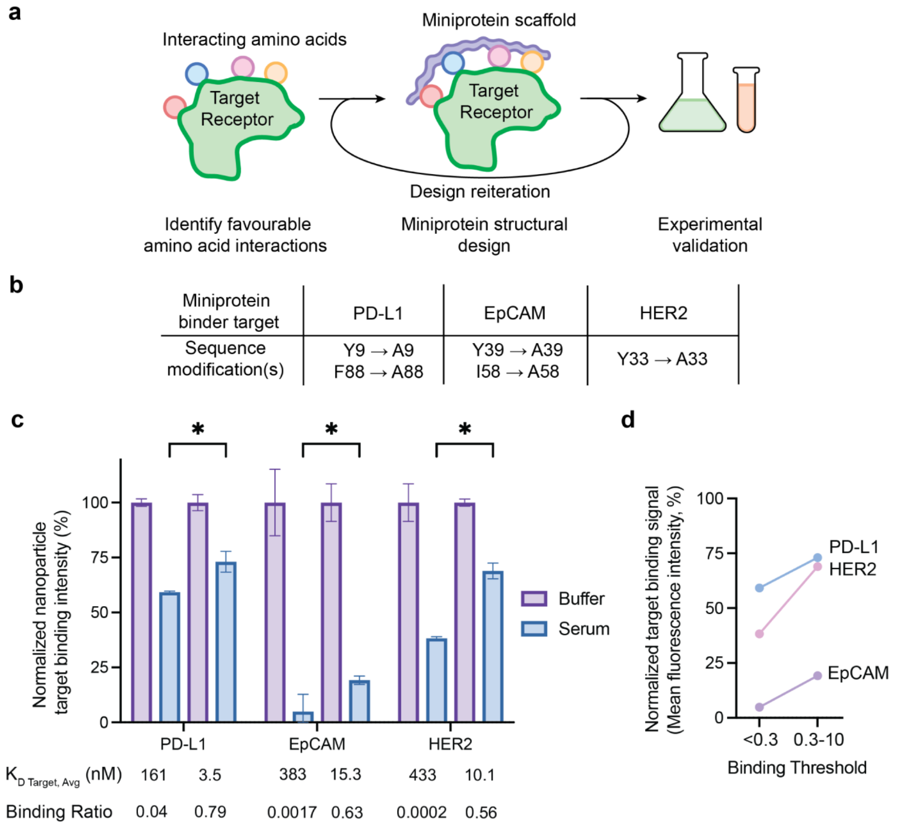

Figure 6. Targeting ligands can be engineered for target binding in serum. (a) Miniprotein binders are engineered to have high or low affinity to target receptors. Favorable interactions are identified between target receptors (green) and individual amino acids (red, blue, pink, and yellow circles). Miniprotein scaffolds (purple) are docked onto the target receptors based on the favorable interactions. Binding motifs are selected and used to guide further iterations of scaffold design. The target protein binding affinities of candidate designs are validated experimentally. (b) A table of the mutations introduced to the miniprotein binder sequences to modulate binding affinity. Mutations are introduced into the designed miniprotein binders to reduce their target protein binding affinity. Sequence modifications indicate the amino acid residue positions that were changed from high target protein affinity binders to create low target protein affinity binders. Miniprotein binders to PD-L1 had a modification in position 9 from tyrosine (Y) to alanine (A) and in position 88 from phenylalanine (F) to alanine (A). Miniprotein binders to EpCAM had a modification at position 39 from tyrosine (Y) to alanine (A) and in position 58 from isoleucine (I) to alanine (A). Miniprotein binders to HER2 had a modification in position 33 from tyrosine (Y) to alanine (A). (c) Fluorescence quantification of miniprotein binder coated liposomes bound to immobilized cognate target receptors in buffer (purple) and in 90%(v/v) human serum (blue). Nanoparticles with miniprotein binders engineered to have high target protein binding affinity had a statistically significant increase in binding to target receptors in serum. The binding signals were normalized to the fluorescence intensity of the bound nanoparticles in the buffer. Statistical significance was evaluated using a multiple unpaired two-tailed *t*-test. $^*p < 0.05$. Exact p values from left to right: $p = 0.007$, $p = 0.038$, $p = 0.00013$. All data points and error bars represent mean ± standard deviation from $n = 3$. (d) A comparison of nanoparticle target binding signal between nanoparticles conjugated with low target ligand binding affinities with a binding ratio $\left(\frac{[T]K_{D\mathrm{serum}}}{[S]K_{D\mathrm{target}}}\right)$ of less than 0.3 and nanoparticles conjugated with high target ligand binding affinities with a binding ratio between 0.3 and 10. PD-L1, HER2, and EpCAM are colored blue, pink, and purple, respectively.

of improving nanoparticle target binding in serum is by engineering ligands to have stronger binding affinities to their target receptor. We illustrate the use of a *de novo* protein design approach. Computationally designed protein binders targeting native receptors are robust and controllable.[33] We created miniprotein binders by varying 65 different amino acid combinations to identify designs with different binding affinities to target receptors.[33] We engineered miniprotein binders to target programmed death ligand 1 (PD-L1), the epithelial cell adhesion molecule (EpCAM), and human epidermal growth factor receptor 2 (HER2) (Figure 6a). We induced mutations in the amino acid sequences to modify the binding affinity of the miniprotein binders. The miniprotein binder mutations for PD-L1 were changing tyrosine (Y) to alanine (A) in position 9 and phenylalanine (F) to alanine (A) in position 88. The weak affinity was 40.6 nanomolar and the strong affinity was 6.5 nanomolar. For the EpCAM binder, mutations were introduced at positions 39 and 58 by modifying tyrosine (Y) to alanine (A) and isoleucine (I) to alanine (A), respectively. The weak affinity was 0.15 micromolar and the strong affinity was 0.3 nanomolar. For the HER2 binder, a mutation was introduced at position 33 by changing tyrosine (Y) to alanine (A). The weak affinity was 0.43 micromolar, and the strong affinity was 10 nanomolar (Figure 6b). Table S1 outlines the sequences and mutations for the attenuated version. We conjugated the low affinity and high affinity miniprotein binders to liposomes. We measured the number of miniprotein binders bound to each nanoparticle design (Supporting Information spreadsheet). We assessed liposome binding to target receptors in serum using the *in vitro* plate assay. The miniprotein binders with weak binding affinity lost 61 to 95% of their target binding in serum compared to that in buffer (Figure 6c). The nanoparticle designs conjugated with weak binding affinity miniproteins had binding ratios of less than 0.3 (Figure 6d). We increased the liposome binding ratios to between 0.3 and 10 by engineering the ligands with a higher target affinity. These engineered ligands resulted in a 20 to 73% increase in liposome binding to target receptors in serum compared to the ligands below the binding threshold (Figure 6c,d).

■ CONCLUSION

We identified a mathematical guideline that can predict nanoparticle target binding in serum. This guideline explains the heterogeneous nanoparticle-target binding efficiencies in serum observed in Mirshafiee et al., Salvati et al., Stordy et al., and Dai et al.'s studies. Nature has evolved to achieve receptor targeting in serum such as in viral systems. Some viruses, such as SARS-CoV-2 and HIV-1, depend on the spike protein ligands on their surface to bind to receptors expressed on host cells in serum.[34−36] Some viruses have also evolved to reduce protein binding by glycosylating their surface proteins, allowing them to effectively evade antibody binding and recognition.[37,38] These modifications may enable viruses to surpass the binding threshold and achieve targeting in serum. By learning from how biological systems have evolved to achieve receptor-mediated binding, we can adapt these appraoches to engineer targeting nanoparticles to achieve targeting in serum.

Our competition model builds on the preliminary *in silico* simulation study of Dell'Orco et al. Their study showed that the target-binding ability of the single nanoparticle design they examined was dependent on the affinity of the target receptor and three different proteins.[6] We experimentally measured the binding affinity of serum proteins for 251 nanoparticles with different materials, sizes, surface charges, and surface chemistries. We quantified these affinities with a single measurement technique using whole human blood serum. We then combined the measured binding affinities with *in vitro* receptor and cell binding data to build, test, and experimentally validate a mathematical guideline that predicts which nanoparticle designs can bind to target receptors. We termed this guideline the binding ratio, $\frac{[T]K_{D\text{serum}}}{[S]K_{D\text{target}}}$. This ratio uses the serum protein binding affinity and target protein binding affinity of a nanoparticle to predict whether it can bind to target receptors. Conceptualizing the process of nanoparticle targeting as a competition between serum and targets led to a nanoparticle target binding model with a high predictive power. In the last 20 years, there has been a stigma that serum proteins always impede nanoparticle ligand binding to cellular receptors. Our study shows that the impact of serum proteins on nanoparticle targeting is not black and white. The impact of serum proteins on ligand binding is dependent on the nanoparticle physicochemical properties and ligand design. Furthermore, we did not profile the serum proteins on the nanoparticle surfaces, but the adsorbed protein may also affect the amount of nanoparticle binding to nontarget receptors. Alternative receptor binding could lead to increased nanoparticle uptake, which is not due to the engineered ligand−receptor interactions.

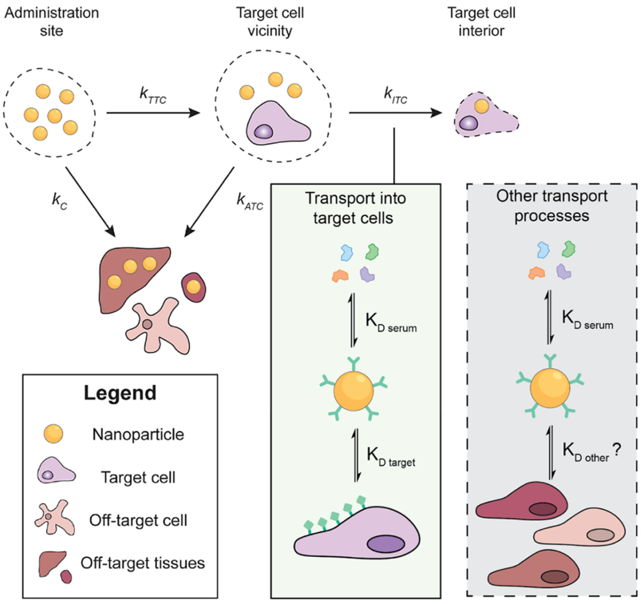

Figure 7. Compartmental model of the processes that control nanoparticle delivery *in vivo*. k_{TTC} is the rate of transport toward a target cell, k_{ITC} is the rate of transport into a target cell, k_C is the rate of clearance, k_{ATC} is the rate of transport away from a target cell, K_D,serum is the serum protein binding affinity, K_D,target is the target protein binding affinity, K_D, other is other cell binding affinities. Adapted with permission and shared first-authorship.[41] Copyright 2022 Elsevier.

The next step is to fully examine the *in vivo* role of serum protein binding affinity and target binding affinity. Pharmacokinetic compartment models have been used to describe nanoparticle distribution *in vivo*.[39−41] Nanoparticles transport through multiple biological compartments before reaching target cells *in vivo*. In nontarget compartments, serum protein binding may cause nanoparticles to be sequestered away from target cells. Determining the transport rate constants between compartments, such as toward target cell, into target cells, away from target cells, and clearance, will allow researchers to design nanoparticles that can transport through the body to the desired location. Neubauer et al. used a three compartment model to profile the pharmacokinetics of paramagnetic liquid perfluoro-carbon nanoparticles *in vivo*.[39] Li et al. developed a pharmacokinetic compartmental model to describe the delivery of inhaled cerium oxide nanoparticles.[40] Wu et al. used a unified compartmental model to conceptualize a general framework to describe nanoparticle delivery *in vivo*.[41] We found that the target and serum protein binding competition is critical when the nanoparticles are in the vicinity of target cells. The effect of serum protein binding affinity and target protein binding affinity on the transport rate into target cells has not yet been accounted for in existing nanoparticle delivery models. We envision our mathematical guideline as a step toward determining the rate constants that describe nanoparticle uptake in cells (Figure 7). Dynamic forces present *in vivo*, such as flow rate and shear forces, may affect the serum protein adsorption binding affinity on the nanoparticle surface. This effect may alter the serum protein binding affinity and therefore the binding ratio. Further studies may be needed to examine the impact of these forces on serum protein adsorption. This study presents the foundational framework required to predict nanoparticle targeting in serum. Evaluating the mathematical description of the roles of serum protein binding affinity and target protein binding affinity enables the prediction of nanoparticle targeting in serum. The binding ratio can be used as a numerical metric to identify nanoparticles for selective targeting in serum.

■ METHODS

Gold Nanoparticle Synthesis. We modified Frens' gold-citrate reduction method to synthesize 15 nm gold nanoparticles (GNPs).[42] 1 mL of 3% (w/v) sodium citrate tribasic dihydrate (Sigma-Aldrich C8532) was added to 100 mL of ultrapure water (Barnstead GenPure 18.2 MΩ cm^{-1}) and brought to a boil in a 250 mL Erlenmeyer flask. 100 μL of 100 g/L gold(III) chloride trihydrate ($HAuCl_4$; Sigma-Aldrich 520918) was added to a rapidly stirring solution. The reaction was stopped by placing the flask on ice for 10 min after the solution turned bright red. 25, 50, 75, and 100 nm GNP were synthesized using modified versions of the Perrault method.[14] 400 mL (25 nm), 300 mL (50 nm), 400 mL (75 nm), or 500 mL (100 nm) of ultrapure water was added to a clean 1 L Erlenmeyer flask and cooled to 4 °C. 0.709 mL (25 nm), 4.545 mL (50 nm), 0.795 mL (75 nm), or 1.994 mL (100 nm) of 44 g/L sodium citrate tribasic dihydrate and 100 g/L HAuCl4 were added to a rapidly stirring solution. 90.32 mL (25 nm), 95 mL (50 nm), 4.72 mL (75 nm), or 6.1 mL (100 nm) of 2.4 nM 15 nm GNPs were then added. 0.709 mL (25 nm), 4.545 mL (50 nm), 0.795 mL (75 nm), or 1.994 mL (100 nm) of 27.5 g/L hydroquinone (Sigma-Aldrich H17902) was rapidly injected into this solution to start the reaction. The reaction was carried out overnight at 4 °C. Tween 20 (Sigma-Aldrich P1379) was added to the GNP the next day to a final concentration of 0.1% (v/v). The GNPs were filled to 12 mL in a 50 mL Falcon tube (BioMart, 110708) and were concentrated by centrifugation at 12,000 × *g* for 15 nm GNP, 8000 × *g* for 25 nm GNP, 700 × *g* for 50 nm GNP, 700 × *g* for 75 nm GNP, and 300× *g* for 100 nm GNP for 1 h. The supernatants were discarded, and the GNPs were transferred to 1.5 mL tubes (Corning 1422215) and washed two more times in a washing solution consisting of 0.02% (w/v) sodium citrate tribasic dihydrate and 0.02% (v/v) Tween 20 in ultrapure water using centrifugation at 8000 × *g* for 25 nm GNP, 800 × *g* for 50 nm GNP, 700× *g* for 75 nm GNP, and 400 × *g* for 100 nm GNP for 30 min. The washed GNPs were combined and stored at 4 °C. The absorbance of the solution was measured by UV−visible spectroscopy (Shimadzu UV1601PC). The GNP concentration was determined using the Beer−Lambert Law. The hydrodynamic diameter was measured by using dynamic light scattering (Malvern Panalytical Zetasizer Nano-ZS).

Gold Nanoparticle Surface Modification with Polymers. The surfaces of GNP were functionalized with one or more of the following polymers: biotin-polyethylene glycol 5000 Da (PEG)-thiol (Creative PEGWorks PBL-8164), methoxy-PEG-SH 550 Da (Creative PEGWorks PLS-607), methoxy-PEG-SH 5000 Da (Sunbright 134874-49-0), methoxy-PEG-SH 2000 Da (Sunbright 134874-49-0), amine-PEG-SH 3000 Da (Rapp Polymere 133000-40-20), amine-PEG-SH 5000 Da (Rapp Polymere 135000-40-20), COOH-PEG-SH 2000 Da (Laysan Bio CM-PEG-SH-2000), COOH-PEG-SH 5000 Da (Laysan Bio CM-PEG-SH-5000), and methoxy-PEG-SH 1000 Da (Laysan Bio MPEGSH1000). Ratios of polymer to nanoparticle were determined by calculating the number of polymers per unit area of the nanoparticle. These ratios are noted in the Supporting Information spreadsheet. Polymers were dissolved in ultrapure water (Barnstead GenPure 18.2 MΩ cm^{-1}) at 1 g/L and combined with GNP prepared at 20 nM in 0.02% (w/v) sodium citrate tribasic dihydrate and 0.02% (v/v) Tween 20. GNP polymer mixtures were incubated in a 60 °C water bath for 1 h. The solutions were washed three times in a washing solution consisting of 0.02% (w/v) sodium citrate tribasic dihydrate and 0.02% (v/v) Tween 20 using centrifugation at 8000 × *g* for 25 nm GNP, 800 × *g* for 50 nm GNP, 700 × *g* for 75 nm GNP, and 400 × *g* for 100 nm GNP for 30 min. The hydrodynamic diameter and concentration of the washed GNP-polymers were determined using dynamic light scattering and UV−visible spectroscopy, respectively.

Gold Nanoparticle Surface Modification with Proteins. The surfaces of 50 nm GNP were functionalized with human apotransferrin (Sigma-Aldrich T2036-500MG), human holotransferrin (Sigma-Aldrich T4132-1G), human serum albumin (Sigma-Aldrich A8763-1G), human immunoglobulin G (Sigma-Aldrich I4506-500MG), cetuximab (Thermo Scientific MA5-47859), trastuzumab (Thermo Scientific MA5-42305), anti-VEGFR (Sino Biological 10012-R002-100), anti-EpCAM (Thermo Scientific 14-9326-82), and anti-PD-L1 (Sino Biological 10084-R015-100). Proteins were first conjugated with orthopyridyl disulfide-PEG-SVA 5000 Da (Laysan Bio OPSS-PEG-SVA-5000-1g) or orthopyridyl disulfide-PEG4-SVA 559.65 Da (Conju-Probe CP-5089) and AZDye 647 NHS ester (Fluoroprobes 1121-100) in a molar ratio of 1 part protein to 3 parts OPSS-PEG-SVA to 2 parts AZDye 647 NHS ester. Proteins were conjugated with this mixture at room temperature overnight. Proteins were washed using Amicon Ultra-0.5 or Ultra-15 centrifugal spin filters with 30k MWCO for apotransferrin, holotransferrin, and albumin (MilliporeSigma UFC500324(Ultra-0.5), UFC903024(Ultra-15)); 100k MWCO for immunoglobulin G, cetuximab, trastuzumab, anti-VEGFR, anti-EpCAM, and anti-PD-L1 (MilliporeSigma UFC510024(Ultra-0.5), UFC9100BK(Ultra-15)). Proteins were washed in 10 mM phosphate, pH 7.4. The absorbance of the solution was measured by UV−visible spectroscopy. The protein concentration was determined using the Beer−Lambert Law. Proteins were combined with nanoparticles in different molar ratios, as noted in the Supporting Information spreadsheet. Conjugations were carried for 2 h at 37 °C in 10 mM phosphate (Sigma-Aldrich S9638, S9390), pH 7.4 for all proteins except immunoglobulin G which was in 10 mM H_2CO_3 pH 9. Conjugated GNP were washed 3 times in 10 mM phosphate pH 7.4 0.02% (v/v) Tween 20 using centrifugation at 1000 × *g* for 30 min at 4 °C. The absorbance and concentration of the washed GNP conjugates were determined as described above. To quantify the number of fluorescent proteins conjugated onto each nanoparticle, proteins were desorbed from the surface by heating nanoparticles at 90 °C for 30 min in a stripping solution (61.75 mM Tris-HCl (BioShop TRS001.1), 0.5% (w/v) sodium dodecyl sulfate (SDS; BioShop SDS003.1), 127.5 mM ethylenediaminetetraacetic acid (Sigma-Aldrich E5134-50G), 2.5% (v/v) glycerol (Invitrogen 15514011), 125 mM dithiothreitol (DTT; BioShop DTT001.5), 1× PBS) before centrifuging at 3000 × *g* for 5 min to pellet the nanoparticles. The protein supernatant was transferred to a 96-well black plate for fluorescence quantification (Tecan Infinite M200 PRO). Standard curves containing the relevant fluorescent labeled protein stocks were prepared and quantified using the same technique.

Gold Nanoparticle Surface Modification with Nucleic Acids. Gold nanoparticles were functionalized with thiolated single-stranded DNA (Integrated DNA Technologies). Sequences are listed in Table S2. Gold nanoparticles were mixed with thiolated DNA strands in the presence of 0.01% SDS based on the following ratios. For 50 nm GNP single stranded DNA was mixed in a stoichiometric ratio of 10,000:1, 20,000:1, and 80 nm GNPs DNA was mixed in a stoichiometric ratio of 40,000:1 or 80,000:1. The DNA was incubated with GNPs for 5 min at room temperature and then adjusted to pH 3 using 100 mM pH 3 sodium citrate tribasic HCl. The mixture was incubated for 30 min at room temperature and subsequently purified by centrifugation at 700 × *g* for 50 nm NP or 500 × *g* for 80 nm GNP. After removing the supernatant, the DNA-functionalized GNP were purified again by centrifugation using 1× PBS containing 0.01% (v/v) Tween 20. The hydrodynamic diameter and optical absorbance of the DNA-functionalized nanoparticles were measured by DLS and UV−vis spectroscopy, respectively, to evaluate stability and conjugation of DNA.

Liposome Synthesis. Liposomes were prepared with the following lipid compositions (mol %): hydrogenated soy phosphatidylcholine (HSPC; Avanti Lipids 840058P) (58.995), cholesterol (Avanti Lipids 700000P) (38), methoxy-polyethylene glycol-phosphatidylethanolamine 2000 Da (mPEG2k-DSPE; Laysan Bio MPEG-DSPE-2000) (1), biotin-polyethylene glycol-phosphatidylethanolamine 5000 Da (biotin-PEG5k-DSPE; Creative PEGWorks PLS-9953) (0.005), azide-polyethylene glycol-phosphatidylethanolamine (azide-PEG5-DSPE, BroadPharm BP-23652) (2), 3,3′-dioctadecyloxacarbocyanine perchlorate (DiO; ThermoFisher Scientific D275) (0.1); HSPC (56.995), cholesterol (38), mPEG2k-DSPE (5), biotin-PEG5k-DSPE (0.005); HSPC (57.995), cholesterol (38), mPEG2k-DSPE (4), biotin-PEG5k-DSPE (0.005); HSPC (58.995), cholesterol (38), mPEG2k-DSPE (3), biotin-PEG5k-DSPE (0.005); HSPC (59.995), cholesterol (38), mPEG2k-DSPE (2), biotin-PEG5k-DSPE (0.005); HSPC (60.995), cholesterol (38), mPEG2k-DSPE (1), biotin-PEG5k-DSPE (0.005); HSPC (61.995), cholesterol (38), biotin-PEG5k-DSPE (0.005); cholesterol (38), mPEG2k-DSPE (1), biotin-PEG5k-DSPE (0.005), azide-PEG5-DSPE (2), 18:0 1,2-stearoyl-3-trimethylammonium-propane (TAP; Avanti Lipids 890880) (58.995), DiO (0.1); HSPC (18.995), cholesterol (38), methoxy-PEG2k-DSPE (1), biotin-PEG5k-DSPE (0.005), azide-PEG5-DSPE (2), TAP (40), DiO (0.1); HSPC (38.995), cholesterol (38), mPEG2k-DSPE (1), biotin-PEG5k-DSPE (0.005), azide-PEG5-DSPE (2), TAP (20), DiO (0.1); HSPC (48.995), cholesterol (38), mPEG2k-DSPE (1), biotin-PEG5k-DSPE (0.005), azide-PEG5-DSPE (2), TAP (10), DiO (0.1); HSPC (53.995), cholesterol (38), mPEG2k-DSPE (1), biotin-PEG5k-DSPE (0.005), azide-PEG5-DSPE (2), TAP (5), DiO (0.1). All lipids were dissolved in 10 mg/mL chloroform (Caledon 3000-1-40). The lipids were mixed in a 20 mL scintillation vial. The lipids were then dried by using a rotary evaporator. The dried lipids were hydrated in 10 mg/mL of 1× PBS (Wisent 311-012-FL). The lipid solution underwent 5 freeze−thaw cycles in liquid nitrogen and a 60 °C water bath. The solution was manually extruded through a 100 nm polycarbonate filter (Whatman 800309) 21 times at 60 °C. The hydrodynamic diameter of the liposomes was characterized using dynamic light scattering.

Liposome Surface Modification with Proteins. The surfaces of liposomes were functionalized with human apotransferrin (Sigma-Aldrich T2036-500MG), human holo-transferrin (Sigma-Aldrich T4132-1G), human serum albumin (Sigma-Aldrich A8763-1G), human immunoglobulin G (Sigma-Aldrich I4506-500MG), cetuximab (Thermo Scientific MA5-47859), trastuzumab (Thermo Scientific MA5-42305), anti-VEGFR (Sino Biological 10012-R002-100), anti-LDLR (Sino Biological 10231-R301-100), anti-EpCAM (Thermo Scientific 14-9326-82), anti-PD-L1 (Sino Biological 10084-R015-100), and hyaluronate 10k amine (Creative PEGWorks HA-321-100 mg). Proteins were first conjugated with dibenzocyclooctyne-PEG5-NHS ester (Vector Laboratories VECTCCTA102P100) and AZDye 647 NHS ester (Fluoroprobes 1121-100) in a molar ratio of 1 part protein to 3 parts DBCO-PEG5-NHS to 2 parts AZDye 647 NHS ester. For antibodies, a molar ratio of 1 part protein to 10 parts DBCO-PEG5-NHS to 2 parts AZDye 647 NHS ester was used. Proteins were conjugated with this mixture at room temperature overnight. Proteins were washed in 1× PBS using Amicon Ultra-0.5 or Ultra-15 centrifugal spin filters with 30k MWCO for apotransferrin, holotransferrin, and albumin; 100k MWCO for immunoglobulin G, cetuximab, trastuzumab, anti-VEGFR, anti-EpCAM, and anti-PD-L1; 3k MWCO for miniprotein binders. Proteins were washed until the filtrate was clear. The absorbance of the solution was measured by UV−visible spectroscopy (Shimadzu UV1601PC). The protein concentration was determined using the Beer−Lambert Law. Proteins were combined with nanoparticles in different molar ratios, as noted in the Supporting Information spreadsheet. Conjugations were carried for 2 h at 37 °C in 1× PBS. Conjugated liposomes were separated from unbound proteins using high-performance liquid chromatography (HPLC) (Agilent 1260 Infinity II) with an Agilent Bio SEC-3 column (Agilent 5190-2513). Elution fractions were collected in a multiwell plate (Greiner 82050-646). The fractions containing liposomes were determined through fluorescence imaging (Tecan Infinite M200 PRO). The hydrodynamic diameter and concentration of the purified liposome conjugates were determined by using dynamic light scattering and fluorescence imaging. To quantify the number of fluorescent proteins conjugated onto each nanoparticle, liposomes were transferred to a 96 well black plate for fluorescence quantification (Tecan Infinite M200 PRO). Standard curves containing the relevant fluorescent labeled protein stocks were prepared and quantified using the same technique.

Iron Oxide Nanoparticle Synthesis. Oleic acid-coated iron oxide nanoparticles (IOOA) were prepared using a previously reported protocol.[43] To functionalize IOOA with poly(ethylene glycol) (PEG) and primary amine groups, 50 mg of IOOA was dissolved in 43 mL of anhydrous toluene (Fisher Scientific AA41464K7) in a three-neck round-bottom flask equipped with a Graham condenser. Subsequently, 50 μL of triethylamine (Sigma-Aldrich 471283-100 ML) was added to the mixture. The flask was sealed with septa, purged with nitrogen, and heated to 100 °C. 0.15 mL portion of (3-triethoxysilyl)propylsuccinic anhydride (SATES) (Gelest SIT8192.6) was then injected into the flask. After 15 min, 281.25 mg of mPEG2K-NH2 (Laysan Bio MPEG-NH2-2000-5GR) in 7 mL of anhydrous toluene was added. An hour later, an additional 75 μL of SATES was introduced, and the reaction was allowed to proceed for 6.75 h. The resulting solution was transferred to a single-neck round-bottom flask and precipitated in hexane. The precipitate was redispersed in anhydrous tetrahydrofuran (THF)(Sigma-Aldrich 401757-100ML), sonicated for 10 min, and again precipitated in hexane (Sigma-Aldrich 178918-4L). The pellet was then resuspended in 10 mL of anhydrous THF and subjected to another 10 min sonication. A mixture of 93.75 mg of mPEG2K-NH2 and 281.25 mg of bis(amine) functionalized PEG (PEG2K-bis(amine) MW 2000) (Sigma-Aldrich 14529-100G-F) in 12 mL of anhydrous THF was added to the suspension. The flask was sealed with septa and purged with nitrogen, and 18.75 mg of *N*,*N*′-dicyclohexylcarbodiimide (DCC) (Sigma-Aldrich D80002-25G) dissolved in 2 mL of anhydrous THF was introduced. The reaction mixture was placed in a sonication water bath at room temperature for 16 h. Following the reaction, the solution was precipitated in hexane, suspended in 20 mL of ethanol (Fisher Scientific BP28184) and sonicated for 10 min. Hexane was again added to precipitate the IONP-PEG-NH2. After removal of the residual hexane, the pellet was dried under nitrogen. Finally, the pellet was resuspended in deionized water (DI), sonicated for 10 min, and purified through size exclusion chromatography using Sephacryl S-200 resin (Cytiva 17058401).

Biotin Conjugation. IONP-PEG-NH2 was first diluted in PBS (pH 7.2) (Thermo Fisher 14190144) to 1 mg/mL and then reacted with NHS-Biotin (Thermo Fisher 20217) at 100:1 biotin:IONP-PEG-NH2 molar ratio. The reaction mixture was incubated at room temperature for 1 h before being purified through size exclusion chromatography using Sephacryl S-200 resin (Cytiva 17058401) in DI water.

Polymer Conjugation. 2 kDa methoxy-polyethylene glycol (mPEG) was conjugated onto the biotinylated iron oxide nanoparticles at densities of 1, 5, 10, 25, 50, 100, and 200 mPEG/nm². Varying mPEG ratios and iron oxide nanoparticles were incubated at 37 °C for 2 h. The iron oxide nanoparticles were washed 6 times using 10 mM phosphate buffer and 0.02% Tween 20 in Amicon Ultra-0.5 centrifugal spin filters with 30k MWCO for 10 min at 10,000 × *g*.

Gas Vesicle Synthesis. Native gas vesicles (GVs) were isolated from *Anabaena flos-aquae* as previously described[44] and stored in 1× PBS. Concentrations were measured by optical density (OD) at 500 nm with a NanoDrop ND-1000 (Thermo Scientific). The following relations were used for stoichiometry calculations: OD 1 GV = 114 pM GV. Stripped GVs were prepared by removing GvpC as previously described.[45] GVs were reacted with 0.2 PEG/nm^2 biotin-PEG-NHS 5000 Da (Nanocs PG2-BNNS-5k-1) overnight and then washed in 1× PBS by centrifugation at 600 × *g* for 30 min. The subnatant was removed and the GVs were resuspended in 1× PBS. This process was repeated three times.

Virus-Like Particle Synthesis. *Microbial Protein Expression and Purification.* The AviTag_I53-50A, I53-40A, AviTag_I53-40B, and I53-50B.4.PT1 proteins were expressed in Lemo21(DE3) (NEB) (New England Biosciences C2528J) in LB which is composed of 10 g of tryptone (Fisher Scientific DF0123-08-4), 5 g of Yeast Extract (Thermo Fisher 212730), and 10 g of NaCl (Fisher Scientific BP358-10) grown in 2 L baffled shake flasks (Bellco 2542-02000). Cells were grown at 37 °C to an OD600 ∼0.8 and then induced with 1 mM IPTG (Teknova I3430). Expression temperature was reduced to 18 °C, and the cells were shaken for ∼16 h. AviTag_I53-50A, I53-40A, and AviTag_I53-40B cells were harvested and lysed by microfluidization using a Microfluidics M110P at 18,000 psi in 50 mM Tris (Sigma-Aldrich 1083155000-5KG), 500 mM NaCl, 30 mM imidazole (Millipore Sigma 1370981000), 1 mM PMSF (Sigma-Aldrich 11359061001), and 0.75% CHAPS (Millipore Sigma C9426-CONF). Lysates were clarified by centrifugation at 24,000 × *g* for 30 min and applied to a 2.6 × 10 cm Ni Sepharose 6 FF column (Cytiva 17531804) for purification by immobilized metal affinity chromatography (IMAC) on an AKTA Avant150 FPLC system (Cytiva). The proteins of interest were eluted over a linear gradient of 30 to 500 mM imidazole in a background of 50 mM Tris pH 8, 500 mM NaCl, and 0.75% CHAPS buffer. I53-50B.4.PT1 cells were harvested, resuspended in 1× PBS, homogenized, and lysed via microfluidization. After initial clarification and discarding of the supernatant, pellets were sequentially washed with 1× PBS containing 0.1% Triton X-100 (pH 8.0) (Millipore Sigma X100-100ML) and 1× PBS with 1 M NaCl (pH 8.0). Protein was then extracted using 1× PBS with 2 M urea (Thermo Fisher 29700) and 0.75% CHAPS (pH 8.0) and applied to a diethylaminoethyl (DEAE) Sepharose FF column. After binding, the column was washed with 1× PBS containing 0.1% Triton X-100 and 0.75% CHAPS (5 CV each, pH 8.0) before the protein was eluted with 1× PBS and 500 mM NaCl (3 CV, pH 8.0). Peak fractions from IMAC or DEAE were pooled, concentrated in 10K MWCO centrifugal filters (Fisher Scientific UFC901096) and sterile filtered (0.22 *μ*m) (Millipore Sigma SLGV013SL), and applied to a Superdex 200 Increase 10/300 (Cytiva 28990944) using 50 mM Tris pH 8, 500 mM NaCl, and 0.75% CHAPS buffer. AviTag_I53-50A, I53-40A, and AviTag_I53-40B eluted at ∼0.6 column volume (CV). I53-50B.4PT1 elutes at ∼0.45 CV. After sizing, AviTag_I53-50A and AviTag_I53-40B were enzymatically biotinylated with BirA (Fisher Scientific NC9204985) and subsequently quantitated with HABA following the manufacturer's protocol (Thermo Fisher 28005).

In Vitro Nanoparticle Assembly. The total protein concentration of purified individual nanoparticle components was determined by measuring absorbance at 280 nm using a UV−vis spectrophotometer (Unchained Laboratories Stunner) and calculated extinction coefficients.[46] Nanoparticles were generated with a molar ratio of the trimeric component to pentameric component of 1:1 by addition in the following order: Biotin_I53-50A or Biotin_I53-40B trimeric fusion protein, followed by additional buffer as needed to achieve the desired final concentration, and last I53-50B. 4PT1 or I53-40A pentameric component with a molar ratio to produce partial displays of biotin on I53-50 and I53-40 nanoparticles (50%, 25%, 15%, 10%, 5% Biotin_I53−50, 5% Biotin_I53-40), both biotinylated and unmodified trimeric components were added together before assembly with pentameric components, still keeping the ratio of *A*:*B* components at 1:1. All Biotin_I53-50 and Biotin_I53-40 *in vitro* assemblies were incubated at room temperature with gentle rocking for at least 30 min before subsequent purification by size exclusion chromatography (SEC) to remove residual unassembled components. Before column application, nanoparticles were sterile filtered (0.22 *μ*m) and purified in 50 mM Tris pH 8, 300 mM NaCl, and 5% glycerol (Sigma-Aldrich G5516-4L) on a Superose 6 Increase 5/150 GL column (Cytiva 29091597). Peak fractions were pooled and sterile filtered (0.22 *μ*m) before nanoparticle size and purity evaluation by SEC-HPLC using a Superose 6 Increase 5/150 GL column on an Agilent 1260 Infinity II high-performance liquid chromatography (HPLC).

Poly(Lactic-*co*-Glycolic Acid) (PLGA) Nanoparticle Synthesis. Three PLGA nanoparticle designs were synthesized with the following formulations: (1) 0.1% (w/w) poly(lactide-*co*-glycolide)-*b*-poly(ethylene glycol)-biotin (Mw

2000-10,000 Da, 50:50 LA:GA) (PLGA-PEG-biotin; PolySciTech AI167), 0.1% (w/w) poly(ethylene glycol) methyl ether-*block*-poly(lactide-*co*-glycolide) (PEG average 2000 Da, PLGA average 10,000 Da, 50:50 lactide:glycolide) (mPEG2k-PLGA, Sigma-Aldrich 913138), 99.8% poly(D,L-lactide-*co*-glycolide) acid terminated (7−17 kDa PLGA, Mw 7000−17,000) (Sigma-Aldrich 719897); (2) 0.1% (w/w) PLGA-PEG-biotin, 10% (w/w) mPEG2k-PLGA, 89.9% (w/w) 7−17 kDa PLGA; (3) 0.1% (w/w) PLGA-PEG-biotin, 25% (w/w) mPEG2k-PLGA, 74.9% (w/w) 7−17 kDa PLGA. 2.5 mg of polymers was synthesized per design. The polymers were dissolved in 10 mg/mL chloroform, combined, and vortexed. The total volume of polymer dissolved in chloroform per design was 250 μL. 2.5 mL portion of 0.1% (w/v) poly(vinyl alcohol) (PVA) (Sigma-Aldrich 363154) was prepared in ultrapure water in a scintillation vial. The solution was stirred rapidly with a magnetic stir bar. 250 μL of PLGA solution was added dropwise to 2.5 mL of 0.1% PVA solution while stirring to yield a PLGA concentration of 0.1 mg/mL. The hydrodynamic diameter of the nanoparticles was determined using dynamic light scattering.

Silica Nanoparticle Surface Modification. 50 nm amine-functionalized silica nanoparticles (nanoComposix SIAN50) and 100 nm amine-functionalized silica nanoparticles (nanoComposix SIAN1000) were reacted with 5 PEG/nm^2 methoxy-PEG-SVA 2000 Da (Laysan Bio MPEG-SVA-2000) and 0.01 PEG/nm^2 biotin-PEG-NHS 5000 Da (Nanocs PG2-BNNS-5k-1) in ethanol at room temperature overnight. Nanoparticles were washed in 0.02% (v/v) Tween 20 in ultrapure water by centrifugation at 21,000 × *g* (50 nm) or 2000 × *g* (100 nm) for 30 min. The supernatant was removed, and the pellet was resuspended with 0.02% (v/v) Tween 20 in ultrapure water. This process was repeated three times. The hydrodynamic diameter of the final purified nanoparticle conjugates was determined through dynamic light scattering.

Polystyrene Nanoparticle Surface Modification. 100 nm amine-functionalized polystyrene nanoparticles (Polysciences Inc., 16586-5) were reacted with 5 PEG/nm^2 2k methoxy-PEG-SVA 2000 Da and 0.01 PEG/nm^2 biotin-PEG-NHS 5000 Da in ultrapure water at room temperature overnight. Nanoparticles were washed in 0.02% (v/v) Tween 20 in ultrapure water by centrifugation at 21,000 × *g* for 30 min. The supernatant was removed, and the pellet was resuspended with 0.02% (v/v) Tween 20 in ultrapure water. This process was repeated three times. The hydrodynamic diameter of the final purified nanoparticle conjugates was determined through dynamic light scattering.

Miniprotein Binder Synthesis. Protein expression was performed using 50 mL of autoinduction media consisting of TBII media supplemented with kanamycin, 2 mM MgSO4, 1× 5052, and grown for 24 h at 37 °C. The cells (NEB, BL21(DE3)) were harvested by spinning at 4000 × *g* for 10 min and then resuspended in lysis buffer (100 mM Tris-HCl, 200 mM NaCl, 50 mM imidazole). Then, the cells were lysed by sonication in a Qsonica Q500 with a 4-pronged horn for 2:30 min at an amplitude of 80%. Soluble fractions were clarified by centrifugation at 4000 × *g* for 30 min. Sample was subsequently purified by affinity chromatography using bed Ni-NTA resin (Qiagen or Thermo Fisher) on a vacuum manifold. A series of 3 washes using wash buffer (20 mM Tris-HCl, 200 mM NaCl, 50 mM imidazole) was performed prior to elution with elution buffer (20 mM Tris-HCl, 200 mM NaCl, 500 mM imidazole). After elution, protein samples were filtered and injected into an autosampler-equipped Akta pure system on a Superdex S75 Increase 10/300 GL column (Cytiva 28-9909-44) at room temperature. The SEC running buffer was 20 mM Tris-HCl, 100 mM NaCl pH 8. We pooled the largest abundance monodisperse peak fractions and concentrated them using spin filters (3 kDa molecular weight cutoff, Amicon, Millipore Sigma) and stored at 4 °C before downstream characterizations. Protein concentrations were determined by absorbance at 280 nm using a NanoDrop spectrophotometer (Thermo Scientific).

Serum Protein Gold Nanoparticle Incubation and Purification. 50 nm gold nanoparticles with and without biotin (0.005 biotin-PEG5k/nm²) and mPEG2k densities of 0, 0.1, 0.25, and 1/nm² were incubated in 5% (v/v) human serum (Sigma-Aldrich H4522) in 10 mM phosphate buffer with 20 mM NaCl and 0.02% (v/v) Tween 20 for 10 min at 37 °C. Nanoparticles were washed with 10 mM phosphate buffer with 20 mM NaCl and 0.02% (v/v) Tween 20 3 times at 1000 × *g* for 30 min. The concentration of gold nanoparticles was measured by using UV−visible spectroscopy.

Serum Protein Isolation from Gold Nanoparticles. Proteins were detached from the nanoparticle surface by combining gold nanoparticles with 1× PBS, 0.5% (w/v) sodium dodecyl sulfate (BioShop SDS003.1), 2.5% (v/v) glycerol (Invitrogen 15514011), 125 mM dithiothreitol (BioShop DTT001.5), 127.5 mM EDTA (BioShop EDT001.500), and 186.75 mM Tris (BioShop TRS001.1). Nanoparticle solution was heated at 90 °C for 30 min. The solution was centrifuged at 3000 ×*g* for 5 min to pellet the nanoparticles. The isolated protein supernatant was transferred to 1.5 mL tubes and was centrifuged once at 10,000 × *g* for 5 min and protein supernatant was collected. The isolated protein supernatant was used for quantification analysis.

Bicinchoninic Acid (BCA) Assay for Adsorbed Protein Quantification on Gold Nanoparticles. To purify the isolated protein solutions and bovine serum albumin standard curves and remove surfactants and reducing agents, 1 mL of ice-cold acetone (Fisher Chemical A18P4) with 10% (w/v) trichloroacetic acid (Sigma-Aldrich T6399) was added and incubated at −20 °C for 1 h. The samples were centrifuged at 21,000 × *g* for 15 min. Supernatant was removed. One mL of ice-cold acetone with 10% (w/v) trichloroacetic acid was again added to the samples and incubated at − 20 °C for 15 min. The samples were centrifuged at 21,000 × *g* for 15 min. Supernatant was removed. One mL of ice-cold acetone was added to the protein pellets and incubated at −20 °C for 15 min. The samples were centrifuged at 21,000 × *g* for 15 min. Supernatant was removed. The addition of adding 1 mL of ice-cold acetone, incubating, centrifuging, and removing the supernatant was repeated 2 more times. The isolated protein samples were allowed to air-dry to evaporate remaining acetone. Samples were then resuspended in 100 μL of 1× PBS and combined with 100 μL of working reagent from the Micro BCA Protein Assay Kit (ThermoFisher Scientific 23225). Samples were incubated at 60 °C for 30 min. The absorbance was read at 562 nm by using a plate reader (Tecan Sunrise).

Polyacrylamide Gel Electrophoresis (PAGE) for Adsorbed Protein Identification on Gold Nanoparticles. Human serum coated gold nanoparticles for each design and a control pure human serum sample were combined with 10 μL of 4× NuPAGE LDS sample buffer (ThermoFisher Scientific NP0007), 5 uL of 1 M dithiothreitol in 1 M Tris. The samples were digested at 90 °C for 30 min. The solution was centrifuged at 3000 × *g* for 5 min to pellet the nanoparticles. The isolated protein supernatant was transferred to 1.5 mL tubes. The samples and protein ladder (ThermoFisher Scientific 10747012) were loaded onto a 4−12% BOLT Bis−Tris mini protein gel (ThermoFisher Scientific NW04120BOX). The gel was run at 200 V for 30 min using a gel electrophoresis system (ThermoFisher Scientific Mini Gel Tank). The gel was removed from the tank and stained in accordance with the ThermoScientific Krypton protein stain protocol. Fluorescent image of the gel was immediately taken using Typhoon FLA 9000 at AF555 laser setting at a 500 V accelerating voltage with 50 μm pixel size.

Biolayer Interferometry Measurement of Serum Protein Binding Kinetics. Biolayer Interferometry (BLI) was used to measure the association and dissociation kinetics of serum and cell surface receptors onto nanoparticles (Sartorius Octet RH16). The buffer type used throughout the measurements for liposomes was 1× PBS with 0.005% (v/v) Tween 20, and BLI buffer consisting of 10 mM phosphate, pH 7.4, 20 mM NaCl, and 0.02% (v/v) Tween 20 for all the other nanoparticle types. Octet streptavidin-coated sensors (Sartorius 18-5019) were submerged in the buffer to hydrate the streptavidin protein on the sensor biosensor for 10 min. The sensors along with the tray were placed in the holder in the instrument. A 384-well black plate was used for the assay. Each well on the plate contained 85 μL of the solution. The measurement was run at 30 °C and under agitation at 1000 rpm. The assay was set up in the following steps: (1) sensor check: sensors move into the buffer to check the instrument status for 1 min. (2) Loading: sensors move into GNP, liposome, silica nanoparticle (SiNP), virus-like particle (VLP), polystyrene nanoparticle (PSNP), poly(lactic-*co*-glycolic acid) nanoparticle (PLGA NP), or iron oxide nanoparticle (FeO NP) solution for nanoparticle loading. (3) Quenching: sensors move in 25 ug/mL solution of biocytin to quench any unbound streptavidin sites and limit nonspecific binding for 5 min. (3) Washing: sensors move into the buffer to remove any loosely bound nanoparticles for 5 min. (4) Baseline: sensors move into the buffer for 1 min. (5) Association: sensors move into 5−7 dilutions of human serum or cell surface receptors to measure protein association onto the nanoparticles. (6) Dissociation: sensors move into the buffer to measure protein dissociation from the nanoparticles. The association and dissociation time was set according to the experimental need (2−10 min). Adeno-associated viruses (AAV) (Progen AAV1 (66V010), AAV2 (66V020), AAV5 (66V050), AAV6 (66V060), AAV8 (66V080), AAVrh10 (66V100), and AAV9 (66V090)) included an additional loading step (1b) where biotin anti-AAVX conjugates (Thermo Scientific 7103522100) or biotin anti-AAV9 (Thermo Scientific 7103332100) conjugates were loaded onto the sensor for 5 min. This was followed by an additional wash step (1c) to remove any loosely bound conjugates prior to AAV loading.

Data Analysis. *Data Processing.* First, the data were processed to correct for background binding, signal drift, and interstep signal discontinuity. The binding curves were subtracted from those of the control sensors. The first control sensor contained nanoparticles with no protein to account for baseline signal drift. The second set of control sensors contained no nanoparticles, which measured the nonspecific binding of proteins to the sensor. Both controls were subtracted from the binding analysis sensors. When the protein solutions were moved into the buffer, there were minor signal shifts, which were corrected such that the beginning of the dissociation phase matched the end of the association phase. A strong binding signal to the sensors results in a negative signal shift. This is because a large change in the optical thickness causes a large wavelength shift, which results in a negative signal. Negative signal shifts were inverted such that the binding signals were positive. All data processing was performed using a Python script, available on GitHub: github.com/chan-lab-code/BLI_processing_fitting.

Data Fitting. After processing the binding curves, a global fit of the entire data set tested at multiple protein concentrations was performed. The fitting equations were constrained such that the binding constants were shared across all of the curves measured at different protein concentrations. This resulted in a single set of binding constants for each nanoparticle design corresponding to a 2:1 heterogeneous binding kinetics model (eqs 1 and 2). The LMfit package was used to fit the binding equations to the data.[47] Basin-hopping, Nelder−Mead, least-squares, or a combination of these methods within LMfit were used to minimize deviation between data and model predictions, resulting in the fitted binding constants. All data fitting was performed using a Python script, available on GitHub: github.com/chan-lab-code/BLI_processing_fitting.

Nanoparticle Receptor Binding Assay. Receptor-coated plates were prepared by incubating polyhistidine-tagged receptors with Ni(2+) chelate-coated 96-well plates (Thermo Scientific 15342) for 1 h at room temperature. Nine pmol of receptor in 100 μL was added to each well. Control wells to account for nonspecific binding were included that were coated with polyhistidine-tagged human serum albumin. Nanoparticles with targeting ligands were prepared as described above. The nanoparticles were fluorescently labeled with an AZDye 647 NHS ester. To determine the level of nanoparticle target binding in serum, nanoparticles were mixed with human serum for a final concentration of 200 pM nanoparticles and 90%(v/v) human serum in 50 μL and then immediately added to the target receptor or control coated wells. To determine the level of nanoparticle target binding in buffer, nanoparticles were mixed with buffer for a final concentration of 200 pM and then immediately added to the target receptor or control coated wells. Nanoparticles were incubated with receptors for 1 h at room temperature, then removed from the wells. The wells were rinsed three times with 100 μL of buffer to remove unbound nanoparticles. Nanoparticles were eluted from the plate with 50 μL of 500 mM imidazole (BioShop IMD508.100) and 1% (w/v) SDS. Nanoparticles were quantified by fluorescence (Tecan Infinite M200 PRO).

Cell Culturing. MDA-MB-468 cells (Cell Biolabs AKR-225) and MDA-MB-231 cells (ATCC HTB-22) were cultured in DMEM (Wisent 319-005-CL) supplemented with 10% fetal bovine serum (FBS; Wisent 098150) and 1% penicillin/streptomycin (Wisent 450-201-E). Both cells were cultured in T175 flasks (Sarstedt 83 3912 002). When the cells reached 80% confluence, they were passaged to a new subculture. Old media was discarded, and the flasks were gently rinsed using 25 mL of 1× PBS. Five mL of trypsin-EDTA (Wisent 325-043-CL) was added to the flask to detach the cells for 5 min at 37 °C. After 5 min, 20 mL of media was added to neutralize the trypsin-EDTA solution. The cell lines were stored at 37 °C and 5% carbon dioxide.

Nanoparticle *In Vitro* Cell Binding Assay. *Nanoparticle-Cell Binding Assay.* MDA-MB-468 cells and MDA-MB-231 cells were seeded in 24-well tissue culture treated plates (Sarstedt 83.3922) at a density of 100,000 cells in 1 mL of complete media per well 1 day prior to running the binding assay. On the day of the assay, the media from each well was discarded and rinsed 2 times using ice cold 1× PBS. The nanoparticles were prepared in two conditions: buffer only and 90% serum only. The nanoparticles in the buffer-only condition were diluted to 200 pM in 10 mM phosphate and 20 mM NaCl for gold nanoparticles and 1× PBS for liposomes. The nanoparticles under the serum-only condition were diluted to 200 pM in undiluted human serum. The nanoparticles prepared in either buffer or human serum on ice were immediately added to each well containing the cells. The nanoparticles were incubated with the cells at 4 °C for 1 h. After 1 h, the nanoparticle solutions were discarded, and the wells were rinsed once using 1× PBS. 0.4 mL of trypsin-EDTA was added to the flask to detach the cells for 5 min at 37 °C. After 5 min, 0.4 mL of complete media was added to neutralize the trypsin-EDTA solution. Cell solutions were transferred to 1.5 mL tubes.

Flow Cytometry. The samples were washed once with 1 mL of blocking buffer consisting of 1× PBS, 0.5% (w/v) bovine serum albumin (BSA) (Sigma-Aldrich A9418), and 2 mM EDTA (BioShop EDT001.500). The samples were stained with Zombie Violet (BioLegend 423114) live/dead stain at 1:200 dilution in 1× PBS on ice for 15 min. The cells were washed once more with blocking buffer, then fixed with 200 μL of 1.6% (v/v) paraformaldehyde (ThermoScientific J61899.AK) in 1× PBS for 30 min on ice in the dark. The cells were washed and stored in the dark in blocking buffer at 4 °C until flow cytometry analysis the following day. Cells were analyzed on a BD LSRFortessa X-20 Cell Analyzer. Flow cytometry data were analyzed using FlowJo v.10.0.7. Live, single cells were identified. Within this population, nanoparticle uptake was quantified as the geometric mean fluorescence intensity for the nanoparticle fluorescence channel.

Statistics. GraphPad Prism version 10.2.3 (347) was used for statistical analysis. The figure captions indicate the statistical test and the corresponding significance.

■ ASSOCIATED CONTENT

Data Availability Statement

All supporting data are available from the corresponding author (W.C.W.C, warren.chan@ntu.edu.sg) upon reasonable request.

Supporting Information

The Supporting Information is available free of charge at https://pubs.acs.org/doi/10.1021/jacs.5c02576.

> Information related to protein quantification, goodness of fit analysis, equilibrium dissociation constants, serum protein binding affinity, gold nanoparticle and liposome receptor binding, flow cytometry gating strategy, alternative hypothesized models for target binding in serum, binding ratio sensitivity and specificity, and peptide and DNA sequences (PDF)
>
> Information related to nanoparticle library physicochemical properties and corresponding kinetic and equilibrium binding constants for serum proteins and target receptors (XLSX)

■ AUTHOR INFORMATION

Corresponding Author

Warren C. W. Chan – *Institute of Biomedical Engineering, University of Toronto, Toronto, Ontario M5S 3E3, Canada; Terrence Donnelly Centre for Cellular and Biomolecular Research, University of Toronto, Toronto, Ontario M5S 3E1, Canada; Department of Chemistry, University of Toronto, Toronto, Ontario M5S 3H6, Canada; School of Chemistry, Chemical Engineering, and Biotechnology, Nanyang Technological University, Singapore 637371, Singapore;* orcid.org/0000-0001-5435-4785; Email: warren.chan@ntu.edu.sg

Authors

Benjamin P. Stordy – *Institute of Biomedical Engineering, University of Toronto, Toronto, Ontario M5S 3E3, Canada; Terrence Donnelly Centre for Cellular and Biomolecular Research, University of Toronto, Toronto, Ontario M5S 3E1, Canada;* orcid.org/0000-0002-1096-3287

Zahra Sepahi – *Institute of Biomedical Engineering, University of Toronto, Toronto, Ontario M5S 3E3, Canada; Terrence Donnelly Centre for Cellular and Biomolecular Research, University of Toronto, Toronto, Ontario M5S 3E1, Canada*

Gabriel D. Patrón – *Department of Computing, Imperial College London, London SW7 2AZ, United Kingdom; Department of Chemical Engineering, University of Waterloo, Waterloo, Ontario N2L 3G1, Canada;* orcid.org/0000-0001-5241-1416

Wei Yang – *Department of Biochemistry, University of Washington, Seattle, Washington 98195, United States; Institute for Protein Design, University of Washington, Seattle, Washington 98195, United States*

Alexander D. Goodson – *Department of Biochemistry, University of Washington, Seattle, Washington 98195, United States; Institute for Protein Design, University of Washington, Seattle, Washington 98195, United States;* orcid.org/0000-0002-5301-3695

Colin Blackadar – *Institute of Biomedical Engineering, University of Toronto, Toronto, Ontario M5S 3E3, Canada; Terrence Donnelly Centre for Cellular and Biomolecular Research, University of Toronto, Toronto, Ontario M5S 3E1, Canada;* orcid.org/0000-0002-3847-3693

Anthony J. Tavares – *Institute of Biomedical Engineering, University of Toronto, Toronto, Ontario M5S 3E3, Canada; Terrence Donnelly Centre for Cellular and Biomolecular Research, University of Toronto, Toronto, Ontario M5S 3E1, Canada*

Guanyou Lin – *Department of Materials Science and Engineering, University of Washington, Seattle, Washington 98195, United States*

Ayden Malekjahani – *Institute of Biomedical Engineering, University of Toronto, Toronto, Ontario M5S 3E3, Canada; Terrence Donnelly Centre for Cellular and Biomolecular Research, University of Toronto, Toronto, Ontario M5S 3E1, Canada*

Bill Ling – *Division of Chemistry and Chemical Engineering, California Institute of Technology, Pasadena, California 91125, United States;* orcid.org/0000-0002-1276-7204

Rashmi Ravichandran – *Department of Biochemistry, University of Washington, Seattle, Washington 98195, United States; Institute for Protein Design, University of Washington, Seattle, Washington 98195, United States*

Derrick R. Hicks − *Department of Biochemistry, University of Washington, Seattle, Washington 98195, United States; Institute for Protein Design, University of Washington, Seattle, Washington 98195, United States*

Mikhail G. Shapiro − *Division of Chemistry and Chemical Engineering, California Institute of Technology, Pasadena, California 91125, United States; Andrew and Peggy Cherng Department of Medical Engineering and Howard Hughes Medical Institute, California Institute of Technology, Pasadena, California 91125, United States;* orcid.org/0000-0002-0291-4215

Miqin Zhang − *Department of Materials Science and Engineering, University of Washington, Seattle, Washington 98195, United States; Institute for Nano-Engineered Systems, University of Washington, Seattle, Washington 98195, United States*

Neil P. King − *Department of Biochemistry, University of Washington, Seattle, Washington 98195, United States; Institute for Protein Design, University of Washington, Seattle, Washington 98195, United States;* orcid.org/0000-0002-2978-4692

David Baker − *Department of Biochemistry, University of Washington, Seattle, Washington 98195, United States; Institute for Protein Design, University of Washington, Seattle, Washington 98195, United States; Howard Hughes Medical Institute, University of Washington, Seattle, Washington 98105, United States*

Luis A. Ricardez-Sandoval − *Department of Chemical Engineering and Waterloo Institute for Nanotechnology, University of Waterloo, Waterloo, Ontario N2L 3G1, Canada;* orcid.org/0000-0001-9867-6778

Complete contact information is available at:
https://pubs.acs.org/10.1021/jacs.5c02576

Author Contributions

[⋈]B.P.S. and Z.S. contributed equally to this work.

Notes

The accompanying code used to process and fit the protein binding data is found at the GitHub repository: github.com/chan-lab-code/BLI_processing_fitting

The authors declare the following competing financial interest(s): W.C.W.C. is a cofounder of Luna Nanotech and consults for Foresite Ventures, METiS Therapeutics, Cystic Fibrosis Foundation, Merck, and Moderna.

ACKNOWLEDGMENTS

W.C.W.C. acknowledges the Canadian Institute of Health Research Grants FDN159932 and MOP-1301431; Canadian Cancer Society Grant 705285−1; Canada Research Chairs Program Grant 950−223824; and Nanomedicines Innovation Network, 2019-T3-01. N.P.K and D.B. acknowledge the Gates Foundation Grant INV-043758 and the Audacious Project at the Institute for Protein Design. M.Z acknowledges the Kuni Foundation Grant A201605. M.G.S. acknowledges the National Institutes of Health Grant RO1-EB018975. Z.S. and C.B acknowledge NSERC for scholarships. Z.S. acknowledges Ontario Graduate Scholarship, Lorne F. Lambier, Q.C. Scholarship, the Cecil Yip Award, and the Barbara and Frank Milligan family for student fellowships and scholarships. B.P.S. acknowledges the Doctoral Completion Award and NSERC CREATE grant for funding support. Additionally, we would like to thank the Nanomedicine Fabrication Center (Nanomed Fab) for their help with the ICP-MS, the Temerty Faculty of Medicine Flow Cytometry Facility for their help with flow cytometry, and The Hospital for Sick Children's Structural & Biophysical Core Facility along with Greg Wasney, James Magnus Jorgensen, and Anthony Semesi for their help with the biolayer interferometer, HPLC, and measurement acquisition. We thank Dina Malounda for help with gas vesicle preparation. The authors wish to thank Jamie L.Y. Wu for reading and improving the manuscript.

REFERENCES

(1) Anselmo, A. C.; Mitragotri, S. Nanoparticles in the Clinic: An Update Post COVID-19 Vaccines. *Bioeng. Transl. Med.* **2021**, *6* (3), No. e10246.

(2) Salvati, A.; Pitek, A. S.; Monopoli, M. P.; Prapainop, K.; Bombelli, F. B.; Hristov, D. R.; Kelly, P. M.; Åberg, C.; Mahon, E.; Dawson, K. A. Transferrin-Functionalized Nanoparticles Lose Their Targeting Capabilities When a Biomolecule Corona Adsorbs on the Surface. *Nat. Nanotechnol.* **2013**, *8* (2), 137−143.

(3) Mirshafiee, V.; Mahmoudi, M.; Lou, K.; Cheng, J.; Kraft, M. L. Protein Corona Significantly Reduces Active Targeting Yield. *Chem. Commun.* **2013**, *49* (25), 2557−2559.

(4) Dai, Q.; Walkey, C.; Chan, W. C. W. Polyethylene Glycol Backfilling Mitigates the Negative Impact of the Protein Corona on Nanoparticle Cell Targeting. *Angew. Chem. Int. Ed.* **2014**, *53* (20), 5093−5096.

(5) Stordy, B.; Zhang, Y.; Sepahi, Z.; Khatami, M. H.; Kim, P. M.; Chan, W. C. W. Conjugating Ligands to an Equilibrated Nanoparticle Protein Corona Enables Cell Targeting in Serum. *Chem. Mater.* **2022**, *34* (15), 6868−6882.

(6) Dell'orco, D.; Lundqvist, M.; Cedervall, T.; Linse, S. Delivery Success Rate of Engineered Nanoparticles in the Presence of the Protein Corona: A Systems-Level Screening. *Nanomed.: Nanotechnol. Biol. Med.* **2012**, *8* (8), 1271−1281.

(7) Wang, X.; Liu, S.; Sun, Y.; Yu, X.; Lee, S. M.; Cheng, Q.; Wei, T.; Gong, J.; Robinson, J.; Zhang, D.; Lian, X.; Basak, P.; Siegwart, D. J. Preparation of Selective Organ-Targeting (SORT) Lipid Nanoparticles (LNPs) Using Multiple Technical Methods for Tissue-Specific MRNA Delivery. *Nat. Protoc.* **2023**, *18* (1), 265−291.

(8) Palanikumar, L.; Al-Hosani, S.; Kalmouni, M.; Nguyen, V. P.; Ali, L.; Pasricha, R.; Barrera, F. N.; Magzoub, M. PH-Responsive High Stability Polymeric Nanoparticles for Targeted Delivery of Anticancer Therapeutics. *Commun. Biol.* **2020**, *3* (1), 95.

(9) Biochem. Biophys. Res. Commun.911979 Abraham, S. A.; Waterhouse, D. N.; Mayer, L. D.; Cullis, P. R.; Madden, T. D.; Bally, M. B. The Liposomal Formulation of Doxorubicin. *Methods Enzymol.* **2005**, *391*, 71−97.

(10) Schoenmaker, L.; Witzigmann, D.; Kulkarni, J. A.; Verbeke, R.; Kersten, G.; Jiskoot, W.; Crommelin, D. J. A. MRNA-Lipid Nanoparticle COVID-19 Vaccines: Structure and Stability. *Int. J. Pharm.* **2021**, *601*, 120586.

(11) Zhao, M.; Lei, C.; Yang, Y.; Bu, X.; Ma, H.; Gong, H.; Liu, J.; Fang, X.; Hu, Z.; Fang, Q. Abraxane, the Nanoparticle Formulation of Paclitaxel Can Induce Drug Resistance by Up-Regulation of P-Gp. *PLoS One* **2015**, *10* (7), No. e0131429.

(12) Sartor, O. Eligard: Leuprolide Acetate in a Novel Sustained-Release Delivery System. *Urology* **2003**, *61* (2), 25−31.

(13) Rosner, M. H.; Auerbach, M. Ferumoxytol for the Treatment of Iron Deficiency. *Expert Rev. Hematol.* **2011**, *4* (4), 399−406.

(14) Cao, Z.-T.; Gan, L.-Q.; Jiang, W.; Wang, J.-L.; Zhang, H.-B.; Zhang, Y.; Wang, Y.; Yang, X.; Xiong, M.; Wang, J. Protein Binding Affinity of Polymeric Nanoparticles as a Direct Indicator of Their Pharmacokinetics. *ACS Nano* **2020**, *14* (3), 3563−3575.

(15) Cedervall, T.; Lynch, I.; Lindman, S.; Berggård, T.; Thulin, E.; Nilsson, H.; Dawson, K. A.; Linse, S. Understanding the Nanoparticle−Protein Corona Using Methods to Quantify Exchange Rates and Affinities of Proteins for Nanoparticles. *Proc. Natl. Acad. Sci.* **2007**, *104* (7), 2050−2055.

(16) Hühn, J.; Fedeli, C.; Zhang, Q.; Masood, A.; Pino, P. D.; Khashab, N. M.; Papini, E.; Parak, W. J. Dissociation Coefficients of Protein Adsorption to Nanoparticles as Quantitative Metrics for Description of the Protein Corona: A Comparison of Experimental Techniques and Methodological Relevance. *Int. J. Biochem. Cell Biol.* **2016**, *75*, 148−161.

(17) Bekdemir, A.; Stellacci, F. A Centrifugation-Based Physicochemical Characterization Method for the Interaction between Proteins and Nanoparticles. *Nat. Commun.* **2016**, *7* (1), 13121.

(18) Sebastiani, F.; Arteta, M. Y.; Lindfors, L.; Cárdenas, M. Screening of the Binding Affinity of Serum Proteins to Lipid Nanoparticles in a Cell Free Environment. *J. Colloid Interface Sci.* **2022**, *610*, 766−774.

(19) Concepcion, J.; Witte, K.; Wartchow, C.; Choo, S.; Yao, D.; Persson, H.; Wei, J.; Li, P.; Heidecker, B.; Ma, W.; Varma, R.; Zhao, L.-S.; Perillat, D.; Carricato, G.; Recknor, M.; Du, K.; Ho, H.; Ellis, T.; Gamez, J.; Howes, M.; Phi-Wilson, J.; Lockard, S.; Zuk, R.; Tan, H. Label-Free Detection of Biomolecular Interactions Using BioLayer Interferometry for Kinetic Characterization. *Comb. Chem. High Throughput Screen* **2009**, *12* (8), 791−800.

(20) Lundström, I. Models of Protein Adsorption on Solid Surfaces. *Prog. Colloid Polym. Sci.* **1985**, *70* (70), 76−82.

(21) Ortega, G.; Mariottini, D.; Troina, A.; Dahlquist, F. W.; Ricci, F.; Plaxco, K. W. Rational Design to Control the Trade-off between Receptor Affinity and Cooperativity. *Proc. Natl. Acad. Sci. U. S. A.* **2020**, *117* (32), 19136−19140.

(22) Dahlquist, F. W. The Meaning of Scatchard and Hill Plots. *Methods Enzym* **1978**, *48*, 270−299.

(23) Yuan, Q.; Lu, X.; Guo, H.; Sun, J.; Yang, M.; Liu, Q.; Tong, M. Low-Density Lipoprotein Receptor Promotes Crosstalk between Cell Stemness and Tumor Immune Microenvironment in Breast Cancer: A Large Data-Based Multi-Omics Study. *J. Transl. Med.* **2023**, *21* (1), 871.

(24) Franovic, A.; Gunaratnam, L.; Smith, K.; Robert, I.; Patten, D.; Lee, S. Translational Up-Regulation of the EGFR by Tumor Hypoxia Provides a Nonmutational Explanation for Its Overexpression in Human Cancer. *Proc. Natl. Acad. Sci. U. S. A.* **2007**, *104* (32), 13092−13097.

(25) Yan, M.; Schwaederle, M.; Arguello, D.; Millis, S. Z.; Gatalica, Z.; Kurzrock, R. HER2 Expression Status in Diverse Cancers: Review of Results from 37,992 Patients. *Cancer Metastasis Rev.* **2015**, *34* (1), 157−164.

(26) Yi, M.; Niu, M.; Xu, L.; Luo, S.; Wu, K. Regulation of PD-L1 Expression in the Tumor Microenvironment. *J. Hematol. Oncol.* **2021**, *14* (1), 10.

(27) Tayama, S.; Motohara, T.; Narantuya, D.; Li, C.; Fujimoto, K.; Sakaguchi, I.; Tashiro, H.; Saya, H.; Nagano, O.; Katabuchi, H. The Impact of EpCAM Expression on Response to Chemotherapy and Clinical Outcomes in Patients with Epithelial Ovarian Cancer. *Oncotarget* **2017**, *8* (27), 44312−44325.

(28) Bax, H. J.; Chauhan, J.; Stavraka, C.; Santaolalla, A.; Osborn, G.; Khiabany, A.; Grandits, M.; López-Abente, J.; Palhares, L. C. G. F.; Hak, C. C. W.; et al. Folate Receptor Alpha in Ovarian Cancer Tissue and Patient Serum Is Associated with Disease Burden and Treatment Outcomes. *Br. J. Cancer* **2023**, *128* (2), 342−353.

(29) Goel, H. L.; Mercurio, A. M. VEGF Targets the Tumour Cell. *Nat. Rev. Cancer* **2013**, *13* (12), 871−882.

(30) Prang, N.; Preithner, S.; Brischwein, K.; Göster, P.; Wöppel, A.; Müller, J.; Steiger, C.; Peters, M.; Baeuerle, P. A.; da Silva, A. J. Cellular and Complement-Dependent Cytotoxicity of Ep-CAM-Specific Monoclonal Antibody MT201 against Breast Cancer Cell Lines. *Br. J. Cancer* **2005**, *92* (2), 342−349.

(31) Gorges, T. M.; Tinhofer, I.; Drosch, M.; Röse, L.; Zollner, T. M.; Krahn, T.; von Ahsen, O. Circulating Tumour Cells Escape from EpCAM-Based Detection Due to Epithelial-to-Mesenchymal Transition. *BMC Cancer* **2012**, *12* (1), 178.

(32) von Zastrow, M.; Kobilka, B. K. Antagonist-Dependent and -Independent Steps in the Mechanism of Adrenergic Receptor Internalization. *J. Biol. Chem.* **1994**, *269* (28), 18448−18452.

(33) Cao, L.; Coventry, B.; Goreshnik, I.; Huang, B.; Sheffler, W.; Park, J. S.; Jude, K. M.; Marković, I.; Kadam, R. U.; Verschueren, K. H. G.; Verstraete, K.; Walsh, S. T. R.; Bennett, N.; Phal, A.; Yang, A.; Kozodoy, L.; DeWitt, M.; Picton, L.; Miller, L.; Strauch, E.-M.; DeBouver, N. D.; Pires, A.; Bera, A. K.; Halabiya, S.; Hammerson, B.; Yang, W.; Bernard, S.; Stewart, L.; Wilson, I. A.; Ruohola-Baker, H.; Schlessinger, J.; Lee, S.; Savvides, S. N.; Garcia, K. C.; Baker, D. Design of Protein-Binding Proteins from the Target Structure Alone. *Nature* **2022**, *605* (7910), 551−560.

(34) Callahan, M. K.; Popernack, P. M.; Tsutsui, S.; Truong, L.; Schlegel, R. A.; Henderson, A. J. Phosphatidylserine on HIV Envelope Is a Cofactor for Infection of Monocytic Cells. *J. Immunol.* **2003**, *170* (9), 4840−4845.

(35) Jayasinghe, M. K.; Gao, C.; Yap, G.; Yeo, B. Z. J.; Vu, L. T.; Tay, D. J. W.; Loh, W. X.; Aw, Z. Q.; Chen, H.; Phung, D. C.; Hoang, D. V.; Prajogo, R. C.; Hooi, L.; Lim, F. Q.; Pirisinu, M.; Mok, C. K.; Lim, K. W.; Tang, S. J.; Tan, K. S.; Chow, E. K.-H.; Chen, L.; Phan, A. T.; Chu, J. J. H.; Le, M. T. Red Blood Cell-Derived Extracellular Vesicles Display Endogenous Antiviral Effects and Enhance the Efficacy of Antiviral Oligonucleotide Therapy. *ACS Nano* **2023**, *17* (21), 21639−21661.

(36) Wyatt, R.; Sodroski, J. The HIV-1 Envelope Glycoproteins: Fusogens, Antigens, and Immunogens. *Science* **1998**, *280* (5371), 1884−1888.

(37) Wei, X.; Decker, J. M.; Wang, S.; Hui, H.; Kappes, J. C.; Wu, X.; Salazar-Gonzalez, J. F.; Salazar, M. G.; Kilby, J. M.; Saag, M. S.; Komarova, N. L.; Nowak, M. A.; Hahn, B. H.; Kwong, P. D.; Shaw, G. M. Antibody Neutralization and Escape by HIV-1. *Nature* **2003**, *422* (6929), 307−312.

(38) Wyatt, R.; Kwong, P. D.; Desjardins, E.; Sweet, R. W.; Robinson, J.; Hendrickson, W. A.; Sodroski, J. G. The Antigenic Structure of the HIV Gp120 Envelope Glycoprotein. *Nature* **1998**, *393* (6686), 705−711.

(39) Neubauer, A. M.; Sim, H.; Winter, P. M.; Caruthers, S. D.; Williams, T. A.; Robertson, J. D.; Sept, D.; Lanza, G. M.; Wickline, S. A. Nanoparticle Pharmacokinetic Profiling in Vivo Using Magnetic Resonance Imaging. *Magnet. Reson. Med.* **2008**, *60* (6), 1353−1361.

(40) Li, D.; Morishita, M.; Wagner, J. G.; Fatouraie, M.; Wooldridge, M.; Eagle, W. E.; Barres, J.; Carlander, U.; Emond, C.; Jolliet, O. Vivo Biodistribution and Physiologically Based Pharmacokinetic Modeling of Inhaled Fresh and Aged Cerium Oxide Nanoparticles in Rats. *Part. Fibre Toxicol.* **2015**, *13* (1), 45.

(41) Wu, J. L. Y.; Stordy, B. P.; Nguyen, L. N. M.; Deutschman, C. P.; Chan, W. C. W. A Proposed Mathematical Description of in Vivo Nanoparticle Delivery. *Adv. Drug Delivery Rev.* **2022**, *189*, 114520.

(42) Frens, G. Controlled Nucleation for the Regulation of the Particle Size in Monodisperse Gold Suspensions. *Nat. Phys. Sci.* **1973**, *241* (105), 20−22.

(43) Park, J.; An, K.; Hwang, Y.; Park, J.-G.; Noh, H.-J.; Kim, J.-Y.; Park, J.-H.; Hwang, N.-M.; Hyeon, T. Ultra-Large-Scale Syntheses of Monodisperse Nanocrystals. *Nat. Mater.* **2004**, *3* (12), 891−895.

(44) Lakshmanan, A.; Lu, G. J.; Farhadi, A.; Nety, S. P.; Kunth, M.; Lee-Gosselin, A.; Maresca, D.; Bourdeau, R. W.; Yin, M.; Yan, J.; Witte, C.; Malounda, D.; Foster, F. S.; Schröder, L.; Shapiro, M. G. Preparation of Biogenic Gas Vesicle Nanostructures for Use as Contrast Agents for Ultrasound and MRI. *Nat. Protoc.* **2017**, *12* (10), 2050−2080.

(45) Lakshmanan, A.; Farhadi, A.; Nety, S. P.; Lee-Gosselin, A.; Bourdeau, R. W.; Maresca, D.; Shapiro, M. G. Molecular Engineering of Acoustic Protein Nanostructures. *ACS Nano* **2016**, *10* (8), 7314−7322.

(46) Gasteiger, E.; Hoogland, C.; Gattiker, A.; Duvaud, S.; Wilkins, M. R.; Appel, R. D.; Bairoch, A. *Proteomics Protocols Handbook*; Humana Press, 2005, 571−607. .

(47) Newville, M.; Otten, R.; Nelson, A.; Stensitzki, T.; Ingargiola, A.; Allan, D.; Fox, A.; Carter, F.; Michał; Osborn, R.; et al. *Lmfit 1.3.2*; Zenodo, 2024.